



Cite this: *Nanoscale*, 2015, **7**, 8663

Heterogeneous catalytic conversion of CO₂: a comprehensive theoretical review

Yawei Li,^{a,b} Siew Hwa Chan^{a,c,d} and Qiang Sun^{*a,b}

The conversion of CO₂ into fuels and useful chemicals has been intensively pursued for renewable, sustainable and green energy. However, due to the negative adiabatic electron affinity (EA) and large ionization potential (IP), the CO₂ molecule is chemically inert, thus making the conversion difficult under normal conditions. Novel catalysts, which have high stability, superior efficiency and low cost, are urgently needed to facilitate the conversion. As the first step to design such catalysts, understanding the mechanisms involved in CO₂ conversion is absolutely indispensable. In this review, we have summarized the recent theoretical progress in mechanistic studies based on density functional theory, kinetic Monte Carlo simulation, and microkinetics modeling. We focus on reaction channels, intermediate products, the key factors determining the conversion of CO₂ in solid–gas interface thermocatalytic reduction and solid–liquid interface electrocatalytic reduction. Furthermore, we have proposed some possible strategies for improving CO₂ electrocatalysis and also discussed the challenges in theory, model construction, and future research directions.

Received 7th January 2015,

Accepted 14th April 2015

DOI: 10.1039/c5nr00092k

www.rsc.org/nanoscale

^aSingapore-Peking University Research Centre, Centre for Research Excellence & Technological Enterprise (CREATE), Singapore 138602, Singapore.

E-mail: sunqiang@pku.edu.cn

^bCenter for Applied Physics and Technology & Department of Materials Science and Engineering, Peking University, Beijing 100871, China

^cSchool of Mechanical & Aerospace Engineering, Nanyang Technological University (NTU), 50 Nanyang Avenue, Singapore 639798, Singapore

^dEnergy Research Institute at NTU (ERI@N), Nanyang Technological University, 1 CleanTech Loop #06-04, Singapore 637141, Singapore

1. Introduction

The increasing concentration of CO₂ in the atmosphere and the resulting global warming have compelled human society to seek effective ways to convert CO₂ into valuable fuels and chemicals to achieve an anthropogenic and sustainable carbon cycle. Among the different approaches to catalytically transform CO₂ to high calorific fuels as ideal energy storage media, thermo-catalysis and electrocatalysis utilizing heterogeneous catalysts



Yawei Li

Yawei Li received his BS degree in 2011 from Peking University, China. He is currently studying towards a PhD degree from the Department of Materials Science and Engineering, Peking University under the supervision of Professor Qiang Sun. His research interests are focused on computational materials design for energy conversion. From October 2014 to April 2015, he visited the Singapore-Peking University Research Centre.



Siew Hwa Chan

Dr Chan is a professor at Nanyang Technological University, Singapore. He graduated with a PhD degree in Internal Combustion Engines from Imperial College London in 1991. His current research is focused on fuel cells and hydrogen technologies. Dr Chan is the recipient of the George-Stephenson Award from IMechE, UK and also the "World's Most Influential Scientific Minds 2014" Award from Thomson Reuters. He is an editorial board member of Fuel Cells and Journal of Power Technologies. Dr Chan is a member of the Management Board of Energy Studies Institute as well as a member of the Advisory Board of Horizon Fuel Cell Technologies.

have become hotly pursued topics due to the fact that the reactions on solid–gas or solid–liquid interfaces are facile and the catalysts exhibit better durability as compared to homogeneous transition metal complexes.

Basically both solid–gas interface thermocatalysis and solid–liquid interface electrocatalysis for CO₂ reduction need to be combined with hydrogen sources, *i.e.*, either atomically activated H* (* denotes surface adsorbed species) or proton–electron pairs (H⁺ + e⁻). Therefore, a good catalyst must have the ability to dissociate hydrogen sources such as H₂O and H₂ into atomic H* or to promote proton–electron transfer with relatively low energy barriers. However, using only a single descriptor to discover better CO₂ reduction catalysts is not enough. Actually, all the reaction intermediates associated with CO₂ reduction need to be carefully scrutinized. Although dramatic progress has been experimentally made in CO₂ catalytic reduction in the last 20–30 years, only limited intermediates such as CO* and HCOO* have been recognized by experimental methods due to the limitation of experimental techniques as well as transient lifetimes of reaction intermediates. Moreover, it is even more troublesome to identify the transition states involved in CO₂ catalytic reduction and constituent elementary reactions using merely kinetic experiment data.

To overcome this inability, theoretical calculations have become powerful tools to investigate reaction mechanisms. Among them, density functional theory (DFT), which computes ground-state energy and its derived properties using electron density instead of wave functions, has substantially reduced computational cost and makes possible calculation of relatively larger systems such as nanoparticles and periodic surfaces. In particular, the first-principles derived energetics, atomic configurations, transition states, energy barriers, and reaction channels can be used to predict the catalytic activities at an atomic level. Furthermore, DFT calculations can also be used to validate the experimental observations or to give explanations in depth. On the other

hand, experimental data can be used to fit the input parameters for successive kinetic Monte Carlo (KMC) or microkinetic simulations. The KMC and microkinetic simulations reveal macroscopic product distribution with temperature, reactant pressure as well as applied potential, which serve as an effective supplement to DFT. In the past few decades, numerous theoretical studies, aiming to identify the real active sites in real-world catalysts and design new candidates, have been performed in the field of catalytic CO₂ conversion. Most of them provide good agreements with the experiments.

Despite the rapid development in theoretical heterogeneous CO₂ catalysis, only limited reviews summarizing the progress in this field are available. Moreover, most of them focused on the reactions that happened at the solid–gas interface. To the best of our knowledge, there have been no literature reviews comprehensively discussing heterogeneous CO₂ conversion that happened at the solid–liquid interface. Herein, we mainly focus on recent theoretical advances in unraveling the reaction mechanisms and designing new catalysts for CO₂ conversion at the solid–gas/solid–liquid interface. The review is organized as follows: in section 2, we outline thermocatalytic CO₂ reduction with respect to different products and possible mechanisms, while electrocatalytic CO₂ reduction at the solid–liquid interface is discussed in section 3 based on both thermodynamic and kinetic solvent models. Section 4 is devoted to discussions on some existing problems and outlooks for the future research in this field.

2. Solid–gas interface thermocatalytic CO₂ reduction

CO₂ is a linear molecule with a large ionization potential and a small electron affinity, and so, compared to donating electrons, accepting electrons from catalyst sites is more feasible for a CO₂ molecule. Therefore, to achieve solid–gas interface thermocatalytic CO₂ conversion, the active sites must have the ability to inject electrons into the antibonding orbital of CO₂. At the same time, as thermocatalytic CO₂ conversion needs H₂ feed gas as a reducing agent, the active sites should possess a moderate ability to dissociate H₂ feed gas into atomic adsorbed H*. Both of these two factors correlate well with the material's electronic structures, such as the d-band center in metals or defect states in oxides. A deeper insight into the underlying factors that control the catalyst performance is thus needed from theoretical efforts. In the past few years, several theoretical reviews have well summarized the theoretical model catalysts that have been used in experiments.^{1,2} We focus here on key intermediates in the different reactions, aiming to identify factors that may improve the thermocatalytic performance. We divide this section into three parts based on three main products detected experimentally, namely methanol (CH₃OH), carbon monoxide (CO) and formic acid (HCOOH). Methane (CH₄) formation is not discussed in this



Dr Qiang Sun is a professor at Peking University, China. He graduated with a PhD degree in Physics from Nanjing University in 1996. His current research interest is in computational materials design for energy and environment applications. These include hydrogen storage, fuel cell, solar energy, CO₂ capture and conversion. He serves as an Associate Editor of Journal of Renewable and Sustainable Energy and is an editorial board member of Materials Transactions and Annals of Materials Science & Engineering.

Qiang Sun

review because of its lower importance in producing portable liquid fuels.

2.1. CO₂ reduction to CH₃OH

CO₂ has been co-fed with CO and H₂ to produce hydrocarbons, C_n ($n > 2$) oxygenates (like alcohols), CH₄ or CH₃OH, depending on catalyst composition and reaction conditions. Among them, liquid products such as methanol are more desirable because of their potential use in alleviating the dearth of fossil fuels. CH₃OH synthesis from CO₂ hydrogenation (CO_{2(g)} + 3H_{2(g)} → CH₃OH_(g) + H₂O_(g)) is a reverse process of methanol reforming. Its standard enthalpy is −49.3 kJ mol^{−1} at 298.15 K. Such a negative enthalpy indicates that the reaction is thermodynamically favorable and that the reaction temperature needs to be controlled at a moderately low level to repel side and reverse reactions.

Among all metal elements, only Cu has been identified to exhibit the ability to catalyze CO₂ hydrogenation to methanol on an industrial scale.^{3,4} In fact, the Cu/ZnO/Al₂O₃ catalytic system is used to convert syngas mixtures (H₂/CO₂/CO) into methanol industrially at moderate pressures (50–100 bar) and temperatures (473–573 K).^{5,6} Despite its wide use, the underlying catalytic mechanism and active sites are still under debate.³ Basically, three main mechanisms have been proposed based on the nuance of interface models and chosen pathways, namely the formate (HCOO^{*}) mechanism, the reverse water–gas shift (RWGS) mechanism and the *trans*-COOH mechanism. In the following, we will present the reaction pathways of the three mechanisms on Cu, as well as their extension to supporting oxides and non-Cu based systems in sections 2.1.1–2.1.3. Mechanisms other than the three main ones are also briefly discussed in section 2.1.4.

2.1.1 HCOO mechanism and its revision. In the HCOO mechanism, formate (HCOO^{*}) is the key intermediate in the reaction pathway. This is based on the fact that earlier X-ray photoelectron spectroscopy (XPS) and temperature programmed desorption (TPD) experiments detected almost a full monolayer of HCOO^{*} on the Cu surface.^{7,8} It has been claimed that HCOO^{*} is the key intermediate for CO₂ hydrogenation to CH₃OH.⁹ The rate-determining step (RDS) is therefore believed to be controlled by the formation and hydrogenation of HCOO^{*}. Accordingly, earlier theoretical studies mainly focused on unveiling low-barrier steps after the formation of HCOO^{*} with respect to different Cu surface structures and Cu–oxide interactions in the industrial Cu/ZnO catalyst. Using *ab initio* molecular orbital (MO) calculations and a simplified cluster model, Kakumoto *et al.* argued that hydrogenation of CO₂ on the Cu/ZnO catalyst primarily happened on the Cu⁺ site with the formation of the HCOO^{*} intermediate bridged on two Cu atoms.¹⁰ Then two surface-adsorbed H^{*} atoms attacked the adsorbed formate, generating dioxomethylene (H₂COO^{*}) and further breaking into formaldehyde (H₂CO^{*}) and hydroxyl (OH^{*}) species. The resulting H₂CO^{*} further reacts with two H^{*}, leading to the formation of methoxy (CH₃O^{*}) and finally to CH₃OH (CO₂ → HCOO^{*} → H₂COO^{*} → H₂CO^{*} → CH₃O^{*} → CH₃OH). The calculated vibrational modes of the intermedi-

ates were in excellent agreement with earlier experimental data. They further found that the catalytically active cationic Cu⁺ sites are mainly located in the interface between metallic Cu and oxide substrate, suggesting a synergistic interaction between Cu and oxides.¹¹

The morphology effect has also been taken into account in DFT calculations. Using a Cu(111) three-layer slab and a Cu₂₉ nanoparticle as calculation models, Yang *et al.* concluded that the Cu₂₉ nanoparticle exhibits superior catalytic activity towards CO₂ hydrogenation to methanol owing to its flexibility and the presence of low-coordinated active Cu sites.¹² These low-coordinated active metal sites could stabilize key intermediates such as HCOO^{*} and H₂COO^{*} and lower the barrier of their hydrogenation. Therefore, design of better catalysts for methanol synthesis should contain enough coordinatively unsaturated Cu sites and positively charged Cu⁺ cations if methanol is produced *via* the HCOO mechanism.

More recently, instead of claiming hydrogenation of HCOO^{*} and H₂COO^{*} and concomitant C–O bond dissociation as rate-limiting steps, Grabow and Mavrikakis¹³ reported that formic acid (HCOOH) rather than H₂COO^{*} was the major hydrogenation product of the HCOO^{*} intermediate, where HCOOH was then further hydrogenated to H₂COOH^{*} species and subsequently underwent C–OH bond dissociation to generate H₂CO^{*}.¹³ We denote it as the revised HCOO (r-HCOO) mechanism. The comparison of relative activation energies for HCOO and r-HCOO mechanisms is illustrated in Fig. 1. The activation barriers for HCOO^{*} hydrogenation to HCOOH^{*} are much smaller than HCOO^{*} to H₂COO^{*}; meanwhile, CH₃O₂^{*} dissociation to CH₂O^{*} is also preferable to H₂COO^{*} dissociation to CH₂O^{*}. Both of these two reaction steps suggest that the r-HCOO mechanism is more likely to dominate on Cu(111). Based on their KMC study, the identified rate-limiting steps included HCOOH hydrogenation as well as CH₃O^{*} formation at low CO₂ flow concentrations or CH₃O^{*} hydrogenation at high CO₂ flow concentrations.

Following the r-HCOO mechanism, Behrens *et al.*⁵ confirmed the main conclusions drawn by Mavrikakis *et al.*, and they also emphasized the importance of the existence of step defects such as Cu(211) in conjunction with alloyed or doped Zn^{δ+} atoms. They found that the higher oxophilicity of Zn would further enhance the stability of oxygen-bound intermediates such as CH₃O^{*}, leading to decreased thermodynamic and kinetic barriers for converting CO₂ into methanol (Fig. 2). More important was the excellent agreement between DFT calculated barriers with the observed activity of their synthesized flat and stepped Zn free and Zn doped nanostructures. All of the above theoretical studies indicate that the r-HCOO mechanism is at least one dominant cause of CH₃OH production from CO₂.

Apart from ZnO, zirconia (ZrO₂) has also been chosen as an efficient promoter and support for the Cu catalyst.^{14–16} It has been found that the cationic Zr site with considerable oxophilicity like Zn could be the key to enhance the CO₂ conversion rate and methanol selectivity.^{14,15} Initially, ZrO₂ acted as the adsorption site for CO₂, while H₂ dissociated on the Cu side,

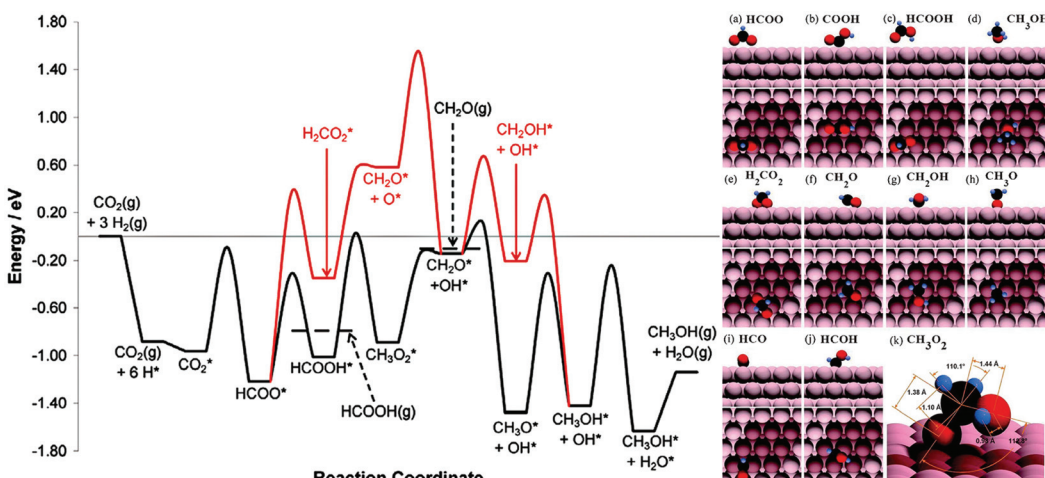


Fig. 1 Potential energy surface and reaction intermediates of CH_3OH synthesis from CO_2 thermocatalytic hydrogenation on $\text{Cu}(111)$ via HCOO and r-HCOO mechanisms [reproduced with permission from (*ACS Catal.*, 2011, **1**, 365–384). Copyright (2011) American Chemical Society].

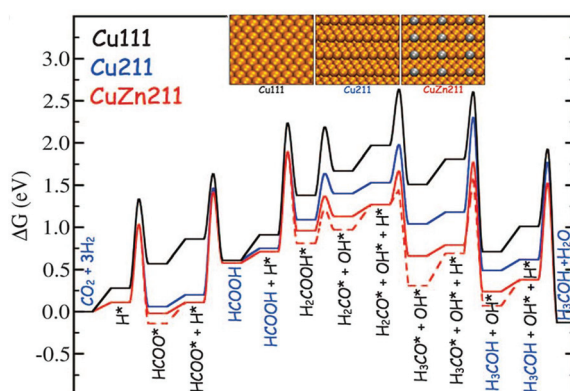


Fig. 2 Gibbs free energy diagram obtained from DFT calculations for CO_2 hydrogenation to CH_3OH on close-packed (black), stepped (blue) and Zn substituted steps (red) [adapted with permission from ref. 5. Copyright (2012) American Association for the Advancement of Science].

emphasizing both the metal and the oxide support effect in modeling.

The role of DFT can also be embodied in modeling of existing non-copper systems. French *et al.* employed the DFT/MM approach and the embedded cluster method to study methanol synthesis on ZnO , the pure oxide substrate without Cu.¹⁷ They found that hydrogenation of the HCOO^* intermediate could generate both HCOOH^* and H_2COO^* . Ye *et al.* applied DFT slab calculations in the investigation of such reactions on the In_2O_3 (110) surface.^{18,19} They suggested that hydrogenation of CO_2 to HCOO^* was more favorable to bicarbonate, and HCOO^* hydrogenation to H_2COO^* was slightly endothermic with an activation barrier of 0.57 eV. The rate-limiting step was hydrogenation of H_2CO^* to H_3CO^* with an activation barrier of 1.14 eV. Both ZnO and In_2O_3 provided oxygen vacancy defects, which would be filled by one of the two oxygen atoms of the

H_2COO^* intermediate. Calculations by the same group revealed that elimination of surface hydroxyl on the Al_2O_3 substrate would facilitate the formation of HCOO^* and inhibit CO^* formation on supported Ni clusters.²⁰ These studies suggest that caution is needed concerning the surface morphology and the adsorption state in modeling oxide substrates where defects may be induced.²¹

In summary, the major dispute in the $\text{HCOO}/\text{r-HCOO}$ mechanism is whether HCOOH^* or H_2COO^* is the preferable hydrogenation product of HCOO^* . The recent experimental and theoretical efforts tend to prove that the r-HCOO mechanism is more favorable.

2.1.2 RWGS mechanism. In contrast to the HCOO mechanism, in the RWGS mechanism CO^* instead of HCOO^* is identified as the key intermediate in methanol synthesis. In other words, CH_3O and CO generations share the same route. CO^* was generated upon the hydrogenation of the COOH^* intermediate, while HCOO^* was regarded as a dead-end spectator species because of the experimental observation that HCOO^* hydrogenation kinetics did not match with that of methanol formation.²² However, theoretical studies reveal that the RWGS route is at least not feasible on pure Cu surfaces. According to the analysis by Yang *et al.*, formyl (HCO^*) was not stable and preferred to dissociate into CO^* and H^* species rather than undergo the reverse pathway on Cu.¹² Therefore, only a small fraction of CO^* generated from the RWGS reaction on Cu nanoparticles could be further converted to methanol and most CO^* would become desorbed on the surface. The selectivity of methanol was therefore significantly hindered.

Promoters or dopants were thus needed to stabilize HCO^* . This is actually the case in industrial examination. Indeed, many different elements have been doped into the Cu-based catalyst to improve its performance on methanol production.³ Based on a combination of DFT and KMC simulations, Yang *et al.*²³ obtained the activity sequence of different metal doped Cu towards methanol synthesis. They found that the

Ni-promoted Cu nanoparticle exhibited the best catalytic performance due to its stabilization of HCO^* .²³ In other words, Ni dopants in Cu nanoparticles could facilitate CH_3OH formation through the RWGS pathway and reduce CO side product generation, as demonstrated by many experimental studies.^{24–26}

Several kinds of fabricated non-copper-based materials also possess notable catalytic activity in transforming CO_2 to CH_3OH via RWGS mechanisms. Theoretical investigations on Cu-free systems were thus stimulated. The DFT method can serve here as an important tool in designing ideal catalytic systems. Liu *et al.*²⁷ used Mo_6S_8 , a structural building block of MoS_2 , to study CO_2 hydrogenation and found that different from periodic MoS_2 which broke C–O bonds of the H_xCO intermediate to form hydrocarbons, Mo_6S_8 catalyzed CO_2 hydrogenation to methanol with moderate activity. CH_3OH was produced via the RWGS route with COOH^* as the intermediate (Fig. 3).

Apart from COOH^* hydrogenation, CO has also been observed to emerge by direct CO_2 dissociation on promoted Cu catalysts. Experimental efforts on $\text{Cu/ZnO/Al}_2\text{O}_3$ and DFT investigation of Cu-ZrO_2 model catalysts both confirmed that CO could be produced by direct CO_2 dissociation ($\text{CO}_2^* \rightarrow \text{CO}^* + \text{O}^*$) without the intermediate COOH^* .^{14,28} The complete reaction network incorporating both HCOO and RWGS mechanisms, as depicted by Tang *et al.*,¹⁴ is shown in Fig. 4. KMC simulations with a large time scale have been used to test the feasibility of CO hydrogenation to CH_3OH with respect to CO_2 under realistic reaction conditions. It was found that a ratio 1 : 1 of CO_2 : CO mixture gas leads to ~2/3 CH_3OH production by CO_2 and ~1/3 by CO,¹³ while pure CO_2 gas resulted in ~85% CH_3OH production by CO_2 and ~15% by CO from CO_2 .

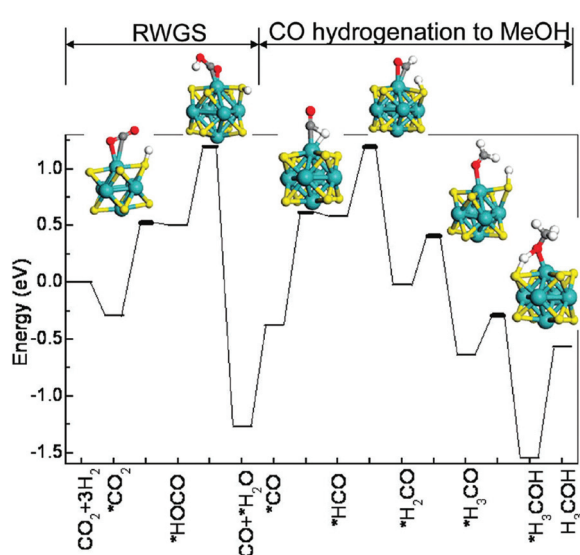


Fig. 3 Optimized potential energy diagram for methanol synthesis from CO_2 and H_2 on a Mo_6S_8 cluster via the RWGS mechanism [reproduced with permission from (*J. Phys. Chem. A*, 2009, **114**, 3888–3895). Copyright (2009) American Chemical Society].

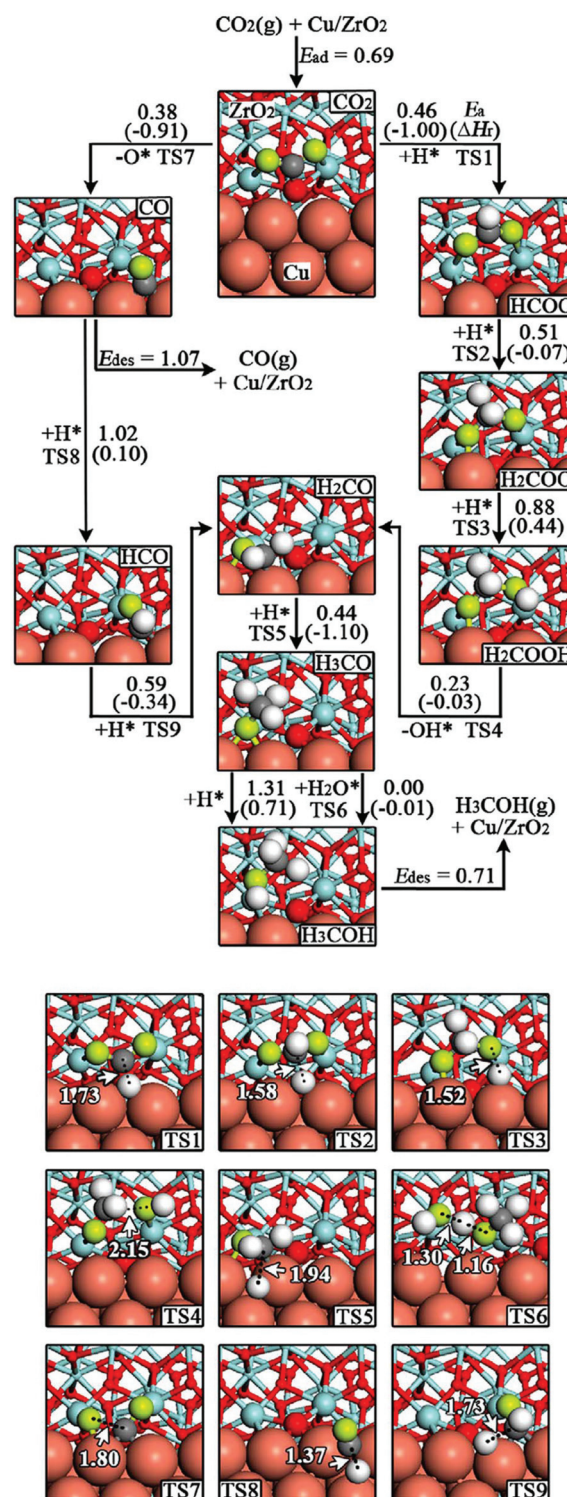


Fig. 4 Reaction network, the intermediates and the transition states for methanol synthesis from CO_2/H_2 over the Cu/ZrO_2 interface [reproduced with permission from ref. 14. Copyright (2009) Elsevier Inc.]

dissociation.¹⁴ The KMC simulations reveal that, under the reaction conditions for CH_3OH synthesis, CO_2 hydrogenation without the generation of the CO^* intermediate is dominant,

while hydrogenation of CO through the RWGS mechanism contributes to a small amount of CH_3OH .

From the above discussions, one can find that the RWGS mechanism cannot be completely ruled out although most theoretical studies claimed that the HCOO^* was the key intermediate and CH_3OH synthesis went through the r- HCOO mechanism. The highest barrier of CO hydrogenation was only slightly higher than that of HCOO^* hydrogenation to CH_3OH . This could account for the observed discrepancy between HCOO^* and CH_3OH formation rates. In the following, we will further show that, in the presence of water molecules in the mixed CO_2/H_2 gas, the CH_3OH production would arguably follow a different mechanism.

2.1.3 *trans*-COOH mechanism: the presence of water. Water is an important factor affecting CO_2 thermocatalytic conversion as found in industrial processes where a considerable amount of gaseous water can be produced by the RWGS reactions. Interestingly, although Tang *et al.*¹⁴ concluded that the r- HCOO mechanism was overwhelming in CH_3OH synthesis from CO_2 , they found that the difficulty in CH_3O^* hydrogenation by surface H^* could be overcome in the presence of H_2O molecules *via* a smaller barrier.¹⁴ Their theoretical investigations have suggested that water might affect reaction barriers of CO_2 hydrogenation, and might even change the preferable reaction routes. In a recent study, Zhao *et al.* indeed proposed an alternative reaction pathway called the *trans*-COOH* mechanism,²⁹ with the generation of *trans*-COOH* rather than HCOO^* as the key limiting step on Cu(111) due to the large barrier of HCOO^* hydrogenation. They found that the presence of water could further lower the formation barrier of *trans*-COOH* and thus promoted CH_3OH synthesis. With the water physisorbed or chemisorbed, the CO_2 hydrogenation barrier was reduced to 0.17 or 0.77 eV, respectively, from 1.17 eV without water molecules (Fig. 5). The *trans*-COOH* would quickly transform into COHOH* and subsequently

COH^* , in contrast to the RWGS mechanism where COOH^* would transform into CO^* and subsequently CHO^* . It is interesting to note that COH^* has been identified as a key intermediate in electrochemical reduction of CO_2 on Cu(111), which will be discussed later. CH_3OH was produced upon the hydrogenation of COH^* , ruling out the existence of both HCOO^* and CO^* intermediates. This study from another perspective explained why trace amounts of water can improve methanol synthesis performance when using a Cu catalyst.

For clarity, in Fig. 6 we summarize the three main reaction mechanisms and the corresponding intermediates during CH_3OH synthesis from a CO_2 thermocatalytic reduction on Cu surfaces. The HCOO mechanism emphasizes the crucial role of the HCOO^* intermediate, while HCOO^* is regarded as a dead-end species in RWGS and *trans*-COOH mechanisms. In addition, whether CO_2 or COOH^* plays a crucial role in CO^* intermediate formation in the RWGS mechanism remains a matter of dispute. In the HCOO mechanism, earlier studies widely accept HCOO^* hydrogenation to H_2COO^* as a rate-determining step,^{10,11} while recent studies suggest HCOO^* hydrogenation to HCOOH^* to be of extraordinary importance.^{5,13} The acidic sites in the interface of metal/metal oxide are believed to significantly enhance methanol productivity and selectivity.^{11,14,16} Promoters (dopants, water, etc.) are supposed to have two primary functions: one is to reduce the barrier of HCOO^* hydrogenation or *trans*-COOH* formation,^{14,29} while the other is to stabilize HCO^* and bind CO^* more strongly to inhibit direct desorption of CO.^{23,30}

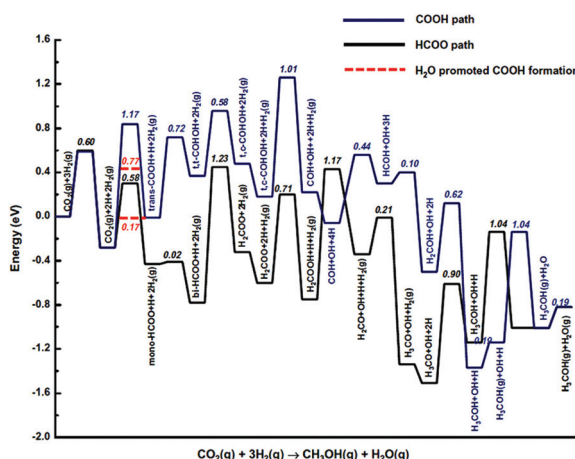


Fig. 5 Potential energy surfaces for CO_2 hydrogenation to CH_3OH on Cu(111) via the HCOO, *trans*-COOH and water promoted *trans*-COOH mechanisms [reproduced with permission from ref. 29. Copyright (2011) Elsevier Inc.]

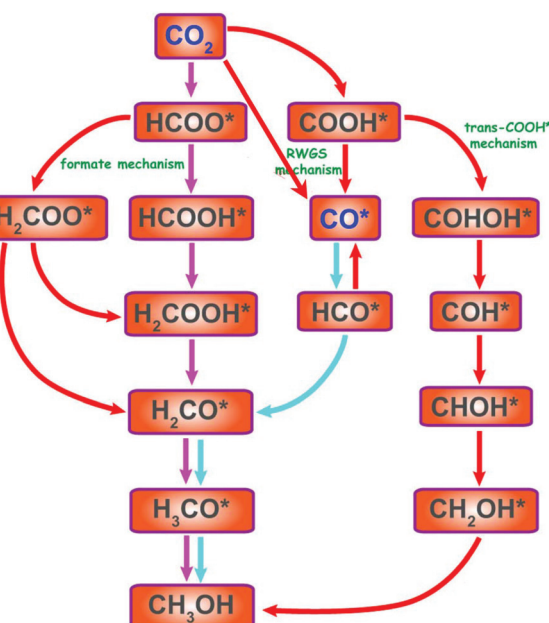


Fig. 6 All possible reaction routes and the corresponding intermediates during methanol synthesis from CO_2 thermo-reduction on Cu. The pink arrows denote the most favorable route for CO_2 reduction while the cyan arrows denote the most favorable route for CO reduction.

2.1.4 Other mechanisms of designed non-Cu catalysts. Mechanisms different from the above-mentioned ones are proposed with the emergence of designed Cu free catalysts. In zeolitic materials containing singly dispersed metal sites, employing DFT in combination with *ab initio* MO theory, Chan *et al.* identified that CO₂ hydrogenation underwent a concerted reaction pathway as CO₂ → HCOOH → H₂CO → CH₃OH with a significantly low barrier,^{31,32} which does not exist in Cu and defect containing oxides. When incorporating alkaline metal cations combined with Ge and N, the Al-based zeolite possessed the best catalytic activity, which is different from conventional acidic zeolite for ethylene hydrogenation. These studies embody that future CH₃OH synthesis catalyst design should not be limited to metal catalysts and oxide catalysts. Metal-organic nanostructures with a similar function as metal-containing zeolites might also be promising candidates for efficient catalyst conversion of CO₂ at low temperatures.

2.2. CO₂ reduction to CO (RWGS reaction)

While Cu-based catalysts are the most extensively utilized for methanol production, many metal elements have been found to be active in catalyzing the CO₂ reduction to CO both experimentally and theoretically. Although Cu-based catalysts have been extensively studied, their applications have been limited as compared to those in methanol synthesis. The main reason is that the RWGS reaction is endothermic and needs higher temperature operation, where Cu-based catalysts suffer from stability issues.

The mechanism of CO₂ reduction to CO on various metal surfaces has also been a subject of dispute for a long time. There are two well established mechanisms named the redox mechanism and the COOH* mechanism. Wang *et al.* performed DFT-GGA calculations of the RWGS reaction on various Cu surfaces according to the redox mechanism, namely, CO₂ dissociates to CO and O before hydrogenation.³³ Their calculations well reproduced the experimentally observed potential diagram, in which the dissociation of CO₂ was the rate-determining step. The dissociation barrier decreased in the order of Cu(111) > Cu(100) > Cu(110). As the geometries of transition states (TS) were found to be similar to the final state (FS), the adsorption energy of surface O* was actually the determining factor. Systematic calculations ignoring the surface H* effect suggested that among Fe(111) to Cu(111) surfaces, Co(111) and Ni(111) exhibited the best catalytic activity in dissociating CO₂ to CO *via* the redox mechanism.³⁴ Vesselli *et al.* studied RWGS reactions that happened on Ni(110), but gave a conclusion that CO was generated from CO₂ *via* the Eley-Rideal (ER) mechanism, with COOH* as an intermediate.^{35,36} This COOH* mechanism is different from the redox mechanism because CO₂ dissociation occurred after its first hydrogenation.

Several supported or free-standing cluster model catalysts were also studied. DFT calculations on molybdenum carbide indicated that adsorbed CO₂ favored the process of splitting into CO and OH species upon approaching an H atom, similar to the redox mechanism.³⁷ However, calculations on various

TiC supported metal catalysts revealed that the major product CO was produced through the COOH* mechanism.³⁸ CO formation on Al₂O₃ supported Ni₄ clusters also passed through an COOH* intermediate and the emergence of surface hydroxyl could further lower the reaction barrier for the RWGS reaction, leading to selectivity towards CO instead of methanol.²⁰

2.3. HCOOH synthesis

HCOOH was not considered as ideal energy storage media initially. However, recently HCOOH has been suggested as a suitable material for hydrogen storage because of a considerably high volumetric capacity of 53.4 g L⁻¹ at standard temperature and pressure (STP). Hydrogen stored in HCOOH can be released on demand by decomposing HCOOH into H₂ and CO₂ at ambient temperature by employing suitable metal catalysts in direct formic acid fuel cells. Therefore, theoretical investigation on catalysts for HCOOH production and decomposition will establish a full energy conversion cycle in hydrogen medium from a computational materials science perspective.

In contrast to many options of metal catalysts such as Pd, Pt, PdAg and PdAu alloys for HCOOH decomposition, heterogeneous thermocatalysts that catalyze HCOOH production effectively remain lacking. DFT calculations were thus primarily conducted to give mechanistic insights rather than materials design and experimental confirmation. Peng *et al.* explored CO₂ hydrogenation to HCOOH by surface H and subsurface H on Ni(110) and Ni(111).^{39,40} They found that both HCOO* and COOH* routes for HCOOH production needed to overcome a large barrier depending on formate hydrogenation or carboxyl formation. Subsurface H might lower the energy barrier and lead the whole reaction from endothermic to exothermic. More recently, Zhang *et al.* hybridized a highly active Lewis base W site into the well Cu-BTC metal organic framework and found that such W sites would catalyze CO₂ into HCOOH effectively.⁴¹

The DFT based screening technique was also applied to identify HCOOH decomposition to H₂ catalysts and to confirm experimental results.⁴² H₂ generation passed through either HCOO* or COOH* depending on metal elements. Turnover frequency (TOF), denoted as the number of products produced per catalytic site per unit time, is often used to characterize the catalyst activity. The TOF for formic acid decomposition over the transition-metal surfaces and the selectivity of H₂ generation were described as functions of CO* and OH* adsorption energies. Pd-Ag alloys exhibited the best catalytic activity and moderate selectivity, and the Cu-Pt alloy was claimed to have better selectivity to suppress the CO generation route in HCOOH decomposition.⁴²

In summary, nanotechnology has had a significant impact on developing ways to control the size, shape, and local composition of Cu and non-Cu based CO₂ thermocatalysts at the nanometer scale. CH₃OH, CO and HCOOH constitute the main products and the underlying mechanisms are well documented. However, to date, much fewer theoretical

investigations have been done in the area of long chain hydrocarbons and higher alcohol thermocatalytic synthesis despite the abundance of experimental practices. We will give further discussions and outlooks in section 4.1.

3. Solid–liquid interface electrocatalytic CO₂ reduction

Compared to solid–gas interface thermocatalytic CO₂ reduction that requires higher operation temperature as well as elevated partial pressure of gaseous reactants, CO₂ reduction that happened on the solid–liquid interface requires merely ambient temperature. Electroreduction of CO₂ is advantageous over other reduction processes that happened in liquids because reactions between CO₂ and electrons (e⁻) can be directly coupled to proton sources to lower the reduction potential. Meanwhile, product distribution can be tuned by changing the applied potential, cathode composition, surface morphology, electrolyte composition, pH value, and so on. Compared to anodes where a proton (H⁺) is generated from the introduced H₂, cathodes where CO₂ receives an e⁻ or proton–electron pair (H⁺ + e⁻) are found to be of more importance in determining the whole reduction process. As a result, earlier experimental efforts mainly focused on which cathode would give a better performance. Metal cathodes are the most intensively investigated because of their low cost and high electric conductivity in liquid electrolytes. Among all the metal cathodes, Cu is the only one found to possess high faradaic efficiency towards CO₂ electroreduction to methane (CH₄) and ethylene (C₂H₄),^{43–47} while Au is characteristic in selectively generating CO.⁴⁸ Such phenomena stimulate theoretical efforts to uncover the underlying factors that dictate strong element dependence.

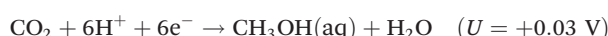
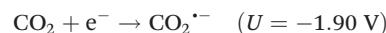
Nevertheless, modeling the electrochemical environment in CO₂ reduction is very challenging. First-principles methods are inadequate in representing the length and time scales associated with a solid–electrolyte interface. Besides, at an electrochemical interface, a charge separation between the electrode metal surface and electrolyte-phase counter ions leads to an electrostatic potential drop, which may affect the local structures and stability of the surface adsorbates. Incorporating these factors into first-principles calculations is thus extremely challenging. As a result, to date various types of model approximations have been developed to theoretically investigate the electrode–electrolyte interface. In the following, we will introduce two kinds of widely-used models as well as their applications to real world electrocatalytic CO₂ reduction. The computational hydrogen electrode model and its applications are presented in section 3.1. In section 3.2, we outline another model denoted as the water solvated and shuttling model. The comparison between experiments and different models is briefly introduced in section 3.3. Note that the models that mimic the solid–liquid interface mainly handle the proton-coupled electron transfer (PCET) steps, which are susceptible to the electrolytes and the applied potential. In contrast, the

C–C coupling steps, which are important in C₂H₄ production, are non-electrochemical and are hardly affected by the solvents. We thus elucidate the two models with respect to mainly CH₄ and CO production and mainly focus on these in sections 3.1 and 3.2. The possible non-electrochemical C–C coupling steps are briefly presented in subsection 3.1.4.

3.1. Computational hydrogen electrode (CHE) model

3.1.1 Origin of CO₂ reduction overpotential. Given the fact that electrocatalytic CO₂ reduction happens at various electrode–electrolyte interfaces, the commonly adopted criterion for evaluating kinetic feasibility is noted as overpotential, which is the potential difference between the reduction potential thermodynamically determined for a half-reaction and the potential at which the redox event is experimentally observed (which means that the measured current starts to increase from 0). In an electrolytic cell, the overpotential determines the amount of energy required to drive a reaction, so it should be as low as possible.

The thermodynamically determined equilibrium potentials for CO₂ reduction to several most common products are listed below:



It is evident that direct electron transfer to CO₂ is much more unfavorable compared to PCET steps. Among different PCET mediated CO₂ reductions, one can see that CO₂ electro-reduction to the simplest hydrocarbon, CH₄, should be feasible at a standard potential of +0.17 V *versus* the reversible hydrogen electrode (RHE). However, a substantial overpotential of about -1.0 V on the Cu cathode is required to perform CO₂ electro-reduction to CH₄ at a high current density. Moreover, at low overpotentials, side products such as CO, HCOOH and H₂ would become dominant. A similar giant overpotential of more than 0.3 eV is also observed on CO₂ electro-reduction to CO on Au electrodes. A recently proposed computational hydrogen electrode (CHE) model serves as a powerful tool in explaining the origin of the overpotential from a purely thermodynamic perspective.

The CHE model was first proposed by Nørskov *et al.* to account for the origin of the overpotential of oxygen reduction reaction (O₂ + 4H⁺ + 4e⁻ → 2H₂O) on a Pt electrode.⁴⁹ The theoretical basis for the validity of the CHE model is that PCET steps that happened in the solution normally possess small kinetic barriers, which are surmountable at room temp-

erature.^{50,51} The reaction kinetics will thus be dictated by merely the free energy difference of each PCET step. The step with the most positive free energy difference is therefore the rate-determining step (RDS).

Apart from omitting PCET kinetic barriers, the kernel idea of the CHE model is that the free energy difference will be quantitatively corrected by the applied potential U . The derivation of free energy correction by U will be presented in the following way: in the RHE, the protons and electrons are in equilibrium with gaseous H₂ at 0 V, all pH values and 1 atm of pressure ($\frac{1}{2}\text{H}_2(\text{g}) \leftrightarrow \text{H}^+(\text{aq}) + \text{e}^-$). Under these conditions, the chemical potential of $\frac{1}{2}\text{H}_2(\text{g})$ is equivalent to that of a proton-electron pair H⁺(aq) + e⁻, namely

$$\frac{1}{2}\mu_{(\text{H}_2(\text{g}))} = \mu_{(\text{H}^+(\text{aq}) + \text{e}^-)}$$

The inclusion of an electron into a proton-electron pair will cause the chemical potential of H⁺(aq) + e⁻ to increase by eU when applying an external bias U :

$$\frac{1}{2}\mu_{(\text{H}_2(\text{g}))} = \mu_{(\text{H}^+(\text{aq}) + \text{e}^-)} + eU$$

When evaluating the free energy difference of a PCET step by calculating the free energy of $\frac{1}{2}\text{H}_2(\text{g})$ rather than that of H⁺(aq) + e⁻, the free energy difference of the step $\Delta G(U)$ is equal to: $\Delta G(U) = \Delta G(U=0) + eU$, where $\Delta G(U=0)$ can be computed using gas-phase free energy data with apposite empirical solvation correction. The corresponding limiting potential U_L at which the free energy difference of RDS turns into 0 is therefore expressed as $U_L = -\frac{\Delta G(U=0)}{e}$.

Hence, under the above-mentioned presumptions and approximations in the CHE model, it is possible to investigate the most favorable mechanism as well as the overpotential of a given electrochemical reaction using only gas-phase acquired free-energy data. The application of the CHE model to the oxygen reduction reaction (ORR) on a Pt cathode has proven that despite the complexity of ORR, when taking the four PCET steps into account, the last PCET step (OH + H⁺ + e⁻ → H₂O) was identified as the rate-determining step and the overpotential is about 0.45 V.⁴⁹ The overpotential value is very close to what is observed experimentally. Inspired by the successful application of the CHE model to ORR and other electrochemical processes and in order to describe why Cu is the most widely used metal electrode for CO₂ electro-reduction to methane and why such a large negative potential is required, Peterson *et al.* performed DFT thermodynamic calculations in conjunction with the CHE model to explore the preferable elementary steps on Cu(211).⁵² The preferred reaction intermediates as well as the free energy difference of each PCET step are illustrated in Fig. 7. They found that the protonation of CO* to CHO* was the key rate-determining elemental step due to its most positive thermodynamic free energy difference of 0.74 eV at 0 V vs. RHE. This means that the whole reaction pathway would be open at a limiting potential of -0.74 V,

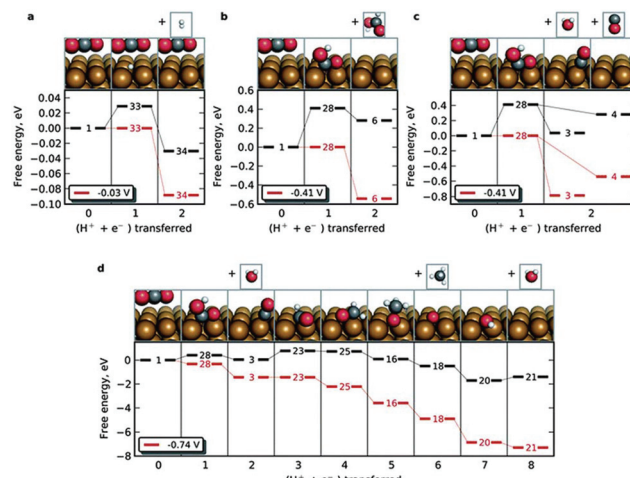


Fig. 7 Free energy diagrams for the lowest energy pathways to H₂, HCOOH, CO and CH₄ in CO₂ electroreduction on Cu(211) [reproduced from ref. 52 with permission from the Royal Society of Chemistry].

equal to an overpotential of 0.91 V, which was in qualitative agreement with the experimental overpotential.⁵²

The CHE model reveals that the overpotential for CO₂ electro-reduction to CH₄ on the Cu cathode results from a notably positive free energy change in the PCET step CO* + H⁺ + e⁻ → CHO*. Using a similar approach, Hansen *et al.* identified that the overpotential for CO₂ electro-reduction to CO on the Au cathode was determined by the free energy change in CO₂ + H⁺ + e⁻ → COOH*,⁵³ and the overpotential value was in agreement with experiments.⁴⁸ One can see that the CHE model, although empirical and using gas-phase free energy calculation data, can show remarkable accordance with earlier experimental studies. That is why most of the state-of-the-art theoretical efforts on CO₂ electro-reduction still adopt the CHE model.

Taking the coverage effect into account, even the product distributions and current changes as a function of the applied potential on the Cu cathode can be fully understood using the purely thermodynamic CHE model. For generations of H₂, HCOOH, CO and CH₄, the corresponding overpotential values change in the following order: the value of H₂ generation is the least, followed by HCOOH and CO and CH₄ generation. That explains why at low applied potential, H₂, HCOOH and CO are the main products on the Cu cathode. Furthermore, it is well known that the generated CO will be adsorbed onto the Cu surface at a high coverage and block the active sites. This results in a decreased production of H₂ and the total current density. Only at the potential where CO* + H⁺ + e⁻ → CHO* becomes exergonic, the CO will be removed and the total current will recover.⁵² The above analyses indicate that the CHE model not only can identify the PCET step where the overpotential is produced, but also can account for many reactions that happened on the cathode.

Besides, the CHE model can be applied to identify stable metal surface phases under realistic electrochemical conditions such as different pH values and applied potentials.

Recent experimental breakthroughs verify the promoting interaction for overpotential reduction on Cu and Sn electrodes by their surface oxides as well as derived metallic nanocrystals.^{54–56} Probing the oxide surface structure and adsorption states for CO₂ reduction intermediates with the DFT technique will thus be helpful for clarification. For example, Nie *et al.* successfully identified O vacancies generated at potential ranges where CO₂ reduction happened on Cu₂O(111),⁵⁷ which accorded well with experimental findings of facile CO₂ reduction on Cu₂O and its derived Cu nanostructures.⁵⁸

Nevertheless, without a full understanding of catalyst electronic structures, the CHE model is still unable to give the reason why Cu and Au are experimentally found to be the best metal cathode for CH₄ and CO production, respectively. Only by combining the well-documented d-band center theory with the CHE model, researchers are able to understand these phenomena *via* a clarified single/double descriptor that depicts a volcano plot. In the next section, we shall explain the basic concepts underlying the volcano plot and present its applications.

3.1.2 Identification of the best metal cathodes—scaling relation and volcano plot. To analyze why Cu is the best cathode candidate for CH₄ production from CO₂ electroreduction, one needs to consider a myriad of metal elements that are commonly used as electrode materials. The considerable positive free energy difference for the process of CO* + H⁺ + e⁻ → CHO* indicates that CO* is stabilized to a larger extent with respect to CHO* on Cu. If there is one kind of metal electrode that stabilizes CHO* in a more pronounced way without strongly binding CO, then the large overpotential for CH₄ generation might be overcome. Nevertheless, there is no such metal cathode that satisfies this criterion because a strong linear correlation between binding energies of CO* and CHO* exists among all the commonly used metal electrodes. Actually, as illustrated in Fig. 8, apart from CO* and CHO* species, other intermediates that bind on metal surfaces through the C

atom also have binding energies that linearly scale with that of CO*. Meanwhile, the adsorption energies of intermediates that bind through the O atom linearly correlate with that of OH*.⁵⁹ It is not surprising to discover such strong linear scaling relations because the position of metal d-band centers affects intermediate adsorption strengths in linear scales.

The free energy difference of a given PCET step A* + H⁺ + e⁻ → B* can be expressed as $\Delta G(U = 0) = \mu_{(B^*)} - \mu_{(A^*)} - \frac{1}{2}\mu_{(H_2(g))}$. As the chemical potential of adsorbate species is directly determined by its binding energy on the metal surface, the free energy difference as well as the limiting potential of each PCET step can be transformed to a function of the binding energies of core adsorbate species, CO* and OH*. That results in volcano-like plots between the limiting potential of RDS and the binding energy of crucial adsorbate species,⁵⁹ as illustrated in Fig. 9, and we call them overpotential volcanoes. The overpotential volcano plots contain a multitude of useful information for better cathode design of CO₂ electro-reduction.

First, the overall predicted limiting potential of the RDS is basically determined by the correlation line between CO* and CHO* because this line stays at the bottommost part of the volcano plots for most part of the binding energy range of CO*. Intermediates that bind to metal with oxygen atoms are in general unable to compete with CO* and CHO* in inducing a more negative limiting potential. The Cu cathode has the best performance for efficient CH₄ generation at high Faradaic yields because it lies near the top of this volcano plot among all the investigated metals. However, the slope of the CO* and CHO* binding energy scale is 0.88, meaning that cathode element change will cause CO* and CHO* to stabilize/destabilize by a similar amount, making the limiting potential of RDS (and therefore the overpotential) alter very little with the cathode material. It is clearly seen from the volcano plot that even if there is a kind of material that lies exactly at the top of the volcano, the limiting potential is still much more negative than -0.5 V. The CHE model derived thermodynamic volcano plot explains why Cu is the best cathode to produce CH₄ and why such a considerable overpotential is needed to initiate CH₄ production.

Second, CO* + H⁺ + e⁻ → CHO* determines the left part of the volcano, while CO₂ + H⁺ + e⁻ → COOH* the right part.

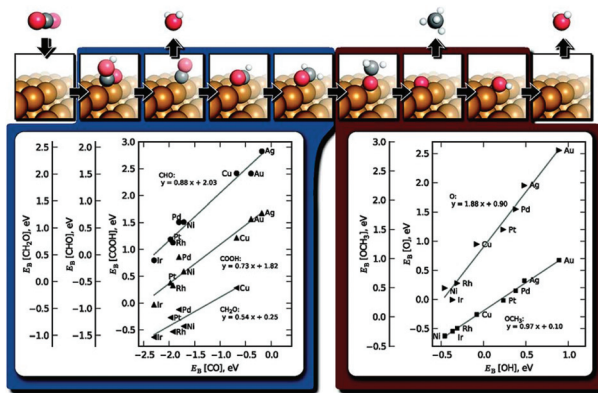


Fig. 8 Adsorption energy scaling of the intermediates in CO₂ electro-reduction on metal surfaces [reproduced with permission from (*J. Phys. Chem. Lett.*, 2012, **3**, 251–258). Copyright (2012) American Chemical Society].

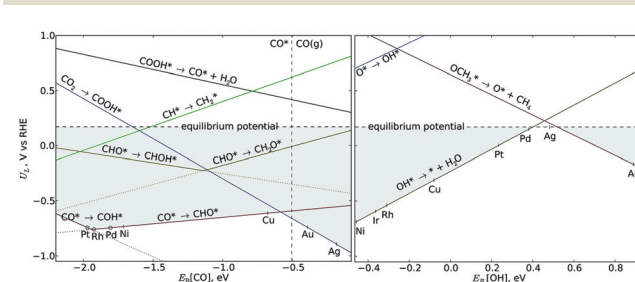


Fig. 9 Overpotential volcano plot of CO₂ electroreduction on metal surfaces [adapted with permission from (*J. Phys. Chem. Lett.*, 2012, **3**, 251–258). Copyright (2012) American Chemical Society].

Interestingly, based on a free energy analysis, it is found that when the CO binding energy is larger than -0.5 V, CO^* prefers to undergo desorption rather than transformation into CHO^* . From the volcano plot in Fig. 9, one can see that the right hand site of the volcano plot coincides with the region where CO undergoes desorption. This explains why Ag and Au cathodes generate CO instead of CH_4 and why Au is the best choice for CO generation among metals. Furthermore, $\text{CO}^* + \text{H}^+ + \text{e}^- \rightarrow \text{CHO}^*$ dictates the overpotential of CH_4 generation on Cu, and $\text{CO}_2 + \text{H}^+ + \text{e}^- \rightarrow \text{COOH}^*$ determines that of CO production on Au and Ag.

Third, the coverage effect on CO_2 reduction and side reactions can be clearly seen on the overpotential volcano. CO molecules generated during CO_2 electro-reduction will block the available metal sites. However, several research groups found that the repulsive interaction between CO^* and H^* as well as between 2CO^* would decrease the binding energy of CO^* and H^* , leading to the point shifting to the right side of the volcano.^{60,61} It is therefore possible to selectively enhance CO_2 reduction but inhibit hydrogen evolution reaction (HER) side reactions in a specific range of the volcano plot.^{61,62}

The overpotential volcano reduces the number of descriptors about overpotential into a single one based on the d-band theory. Combining the CHE model and microkinetic simulation, another kind of volcano plot can be generated, which is called an activity volcano. In contrast to the microkinetic simulations applied in solid–gas interface thermocatalysis, the kinetic barriers of PCET steps are omitted as indicated in the CHE model. Instead, the pre-exponential factors in the microkinetic simulations of electrocatalysis are fitted based on experimentally measured current densities. The corresponding PCET reaction rate constants are thus determined only by the free energy differences and the applied potential. Given the complexity of eight PCET steps contained in CO_2 reduction to CH_4 , only the CO_2 electro-reduction to CO is investigated by Hansen *et al.* in this approach.⁵³

The corresponding activity volcano at a specific applied potential is shown in Fig. 10, where the partial current density is a function of both COOH^* and CO* binding energies that scales with the d-band center among metal cathodes, and the COOH^* – CO^* binding energies are essentially linearly correlated. The activity volcano plot fits the experiments well and explains why Au and Ag possess the best performance in catalyzing CO_2 to CO and why it is difficult to improve the performance of metal cathodes to a larger extent.

The scaling relations and volcano plots unveil the electronic structure factors that hinder the improvement of metal cathode performance. In the following, we will summarize several approaches to improve the cathode catalytic performance based on tuning the electronic structure of the cathode.

3.1.3 Strategies to improve the catalytic performance. The volcano plots derived from the CHE model not only uncover the determining PCET steps that lead to the large overpotential, but also reveal that the notable overpotentials irrespective of cathode metal choice originate from a strong linear correlation between the adsorbates that bind to the metals *via* the

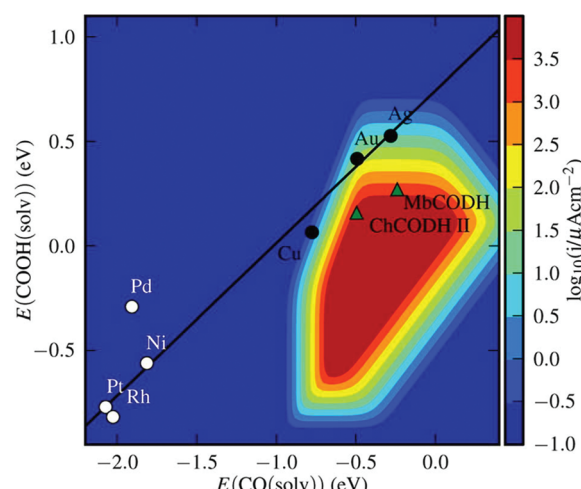


Fig. 10 Activity volcano plot and scaling relation of CO_2 electroreduction to CO on metal surfaces [reproduced with permission from (*J. Phys. Chem. Lett.*, 2013, **4**, 388–392). Copyright (2013) American Chemical Society].

same atom. Given the fact that the CHE model is an empirical approximation to the solid–liquid interface and actually adopts gas-phase DFT results, it indicates that the d-band center theory of the metal surface state is not only validated in solid–gas interface thermocatalysis^{63,64} but also effective in solid–liquid interface electrocatalysis.

To seek suitable cathodes that alleviate the large overpotential in CO_2 electro-reduction, materials that reside closer than Cu or Au to the top of metal overpotential volcano are certainly a kind of choice. However, a more intriguing idea is that the adsorption strengths of PCET intermediates should not conform to the scaling relations found on metal cathodes. It implies that promising cathode materials search should not be limited to pure metals as the traditional d-band center theory is always applicable therein. To the best of our knowledge, several strategies abiding by the two ideas have been proposed in the literature as described below.

3.1.3.1. Tuning the surface geometry and size effect. Although Cu is found to have the best performance for CH_4 generation and Au for CO production, different facets would exhibit different intermediate binding energies because of the different positions of the d-band center. By directly tuning the geometry and nanoparticle size, the overpotential might be further lowered compared to the model Cu(111) and Au(111) surface. Durand *et al.* studied the surface structure effect on Cu electrodes and found that the stepped Cu(211) surface was the most active surface in producing CH_4 .⁶⁵ Lim *et al.* proved that a supported Cu₅₅ nanoparticle with more coordinatively unsaturated edges and vertices could also decrease the overpotential needed compared to the Cu(111) terrace.⁶⁶ Zhu *et al.*, on the other hand, found that the enriched ratio of edge sites in size selected Au nanoparticles account for COOH^* stabilization and overpotential diminish with respect to Au(111) and Au(211).⁶⁷ The performances of both Cu and Au nanoparticles

have been well characterized in subsequent experimental studies,^{67–69} indicating that further efforts at morphology control are underway.

3.1.3.2. Increasing the oxophilicity of the active sites.⁵⁹ CO* tends to bind to the active sites in an upright configuration with respect to the C atom. In contrast, CHO* and COOH* bind to the active surface sites with the C=O bond nearly parallel to the surface in some cases. When the designed catalyst has more sites with higher oxophilicity, the CHO* and COOH* intermediates will bind to the active sites stronger with both C and O atoms whereas the CO* intermediate will not be affected. The strong binding of CHO* and COOH* will break the linear correlation between adsorbates, making the designed materials reside closer to the top of the current density volcano as well as possess lower overpotentials.

3.1.3.3. Designing materials that bind different adsorbates with different element sites. In electrocatalytic CO₂ reduction on metal cathodes, crucial intermediates such as CO*, COOH* and CHO* will bind to the surfaces with the same C atom and at the same element sites. Based on the d-band center theory, the nearer the d-band center is to the Fermi level, the stronger the adsorbate–metal interaction is. The strong correlation between different adsorbates is therefore not unexpected. By decoupling these intermediates into distinct adsorption sites composed of different elements, the conventional scaling relations that impose limitations on metal cathodes will not be valid while new scaling relations will be constructed, which might pass through the top of the activity volcano.

Enzyme arrays immobilized on metal cathodes based on such a design principle exhibit much higher current densities than traditional metal cathodes at the same applied potential. For example, Parkin *et al.*⁷⁰ discovered that the enzyme ChCODH I immobilized on a graphite edge electrode could convert CO₂ to CO with a notable current density of 0.05 mA cm² at only a 0.15 V overpotential. By theoretically investigating the C cluster structure of the CODH enzyme that contains M₄S₄/M₄S₅ (M = Ni, Fe) in a cubane structure, Hansen *et al.*⁵³ and Varley *et al.*⁷¹ identified that the C atom of COOH* and CO* intermediates bound to the S site and the M site, respectively. The different element composition of the active binding sites gave rise to a unique scaling line of adsorption energies between CO* and COOH*, and the line directly passed through the center of the activity volcano (Fig. 11).

Metal dichalcogenides are another example. Based on first-principles calculations, Chan *et al.* identified that COOH* and CHO* intermediates preferred to adsorb on the S or Se sites at the edge of MoS₂/MoSe₂, whereas CO* was likely to bind to the Mo sites (Fig. 12a).⁷² The enhanced adsorption of COOH* and CHO* on S/Se sites accounted for the lowered overpotential and a significant improvement in catalytic activity. Electronic structure analyses of MoS₂ performed by Tsai *et al.*⁷³ revealed that there was a negative correlation between adsorbate–edge Mo binding and the d-band center of edge Mo atoms, similar to that between adsorbate–metal binding and the d-band center of surface metal on metal cathodes. Interestingly, they observed a positive correlation between adsorbate–edge

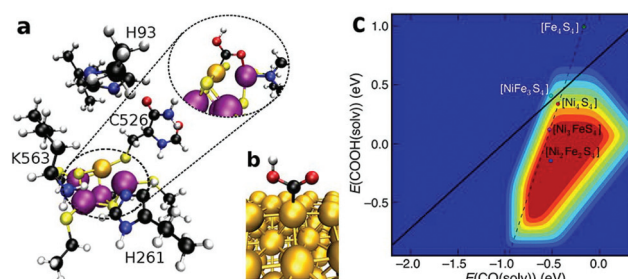


Fig. 11 Activity volcano plot and scaling relation of CO₂ electroreduction to CO. The binding of COOH with sulfur in CODH enzyme (left) leads to a unique scaling relationship that passes through the center of the activity volcano (right) [adapted with permission from (*J. Phys. Chem. Lett.*, 2013, 4, 388–392) and (*ACS Catal.*, 2013, 3, 2640–2643). Copyright (2013) American Chemical Society].

S binding and the d-band center of edge Mo atoms (Fig. 12c), which was believed to lead to the unique location of intermediate adsorption strengths as revealed in Fig. 12b.⁷³ Indeed, a recent experimental investigation confirmed that the edge-rich MoS₂ in 4% EMIM-BF₄ ionic liquid had the lowest onset overpotential (54 mV), the highest current density (65 mA cm²) and an extremely high Faradaic efficiency (~98%) at higher overpotential (0.654 V) reported to date in CO₂ electroreduction to CO.⁷⁴ Both CODH enzymes and metal dichalcogenides possess edge S, suggesting that incorporation of new materials containing group 16 elements is an effective way to break the scaling limitations that existed in pure metals.

Apart from new cathodes that are not based on metals, p-block element doped in metal cathode surfaces will also disrupt the correlation between adsorption energies of PCET intermediates. Lim *et al.* found that the d-block dopants in the Ag cathode would not decouple the correlation between the d-band center of Ag and binding energies of CO and COOH, while the p-block dopants gave rise to a significant decoupling.⁷⁵ Among the different p-block elements, S and As dopants both withstood subsurface diffusion and lessened the overpotential to a larger extent as could be seen in the center of the overpotential volcano plot. The stronger binding of *COOH at the S/As site than CO at the fcc hollow site was attributed to the least energy cost for singly occupied p_z orbital generation as well as the largest covalent bonding energy gain (Fig. 13). This pioneering research suggests that active site engineering is also practically effective in traditional metal cathodes.

3.1.3.4. Inserting organometallic porous nanomaterials. It has been well established that organometallic Co-porphyrin is able to homogeneously catalyze CO₂ electro-reduction both experimentally and theoretically.^{76–78} Extending this kind of structure to a periodic counterpart, Tripkovic *et al.* systematically studied various porphyrin like metal-graphene divacancy (GDV) structures.⁷⁹ The scaling relationship changed substantially as compared to the extended metal surfaces, resulting in an overpotential decrease in several kinds of metal-GDV such

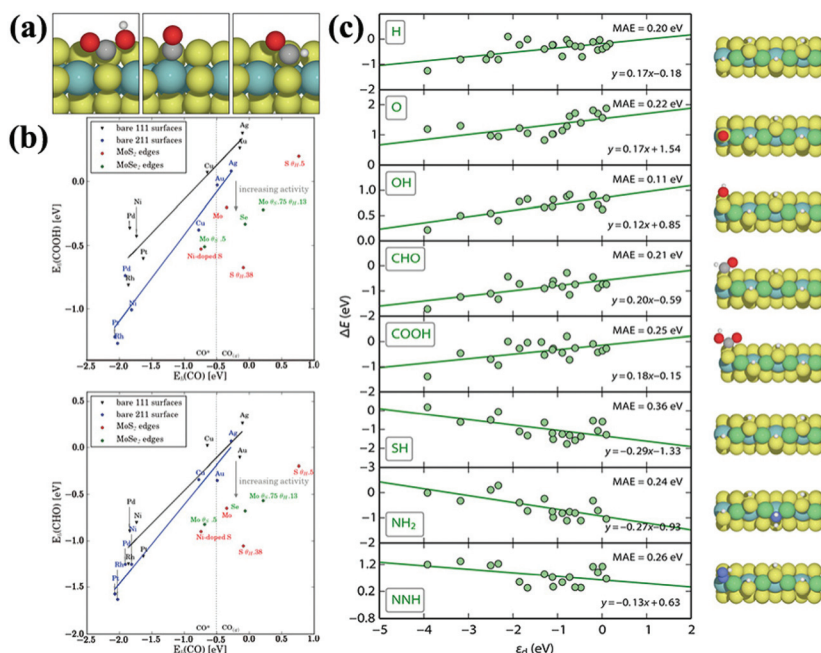


Fig. 12 Adsorption configurations of COOH*, CO* and CHO* on MoS₂ edges (a); deviation of scaling relationships for metals on MoS₂ and MoSe₂ (b); reverse correlations between adsorbates on S and adsorbates on Mo with respect to the Mo d-band center (c) [adapted with permission from ref. 72. Copyright (2014) WILEY-VCH Verlag GmbH & Co. KGaA, Weinheim; adapted with permission from (*J. Phys. Chem. Lett.*, 2014, **5**, 3884–3889). Copyright (2014) American Chemical Society].

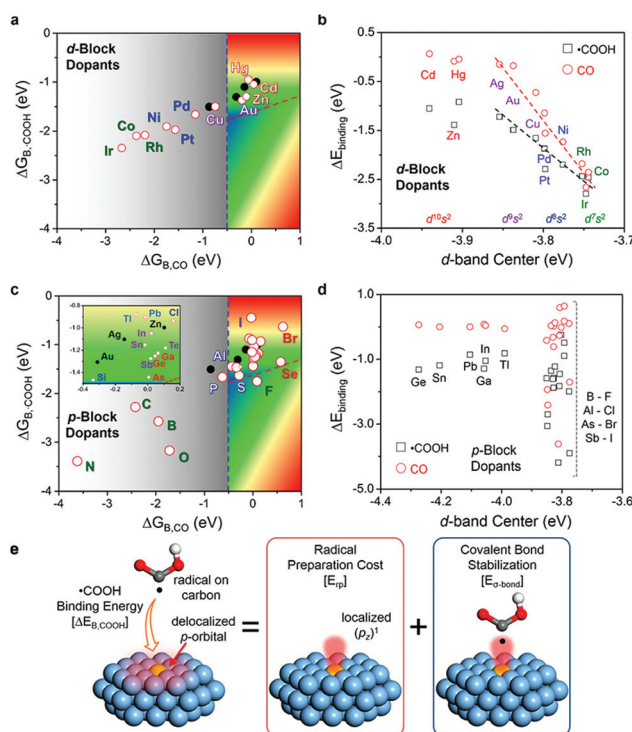


Fig. 13 Variations of COOH and CO stabilization depending on the dopants and their correlation with the d-band center (a-d); schematic diagram of the COOH binding mechanism on p-block dopants (e) [reproduced with permission from (*J. Am. Chem. Soc.*, 2014, **136**, 11355–11361). Copyright (2014) American Chemical Society].

as Rh-GDV. The unique scaling relationship arose from atomic-like sharp d-band peaks observed in metal-GDV structures.

Through our elucidation using PCET steps in CH₄ and CO production from CO₂ electrocatalysis as subjects, one can find that the CHE model and overpotential or activity volcano plots not only uncover the electronic factors that determine the overpotential that existed among metal cathodes, but also provide useful guidance for better catalyst design. For a better understanding of some crucial reaction intermediates and the origins of reaction overpotential, in the next part, a brief introduction is given for the CHE model extended to C₂ products such as C₂H₄.

3.1.4 Mechanism for C₂H₄ production. CO₂ electro-reduction to C₂H₄ shares some similar features with that to CH₄ where CO* has been identified as a crucial reaction intermediate. Nevertheless, C₂H₄ formation includes non-electrochemical C–C coupling steps that cannot be handled by the CHE model. Montoya *et al.* carried out a first-principles theoretical study on C–C coupling in CO₂ electro-reduction on the Cu(211) surface.⁸⁰ They found that the kinetic barriers for 2 CO* dimerization were kinetically unfavorable and protonation of CO* to form CHO* must become exergonic before favorable kinetics could be achieved. Their results accounted for the similar onset potentials for CH₄ and C₂H₄ in experiments. Furthermore, the experimental trend of higher C₂H₄ selectivity at onset potentials of CH₄ and C₂H₄ was also corroborated by the DFT results that C–C coupling possessed lower barriers at low overpotentials, while CHO* hydrogenation was

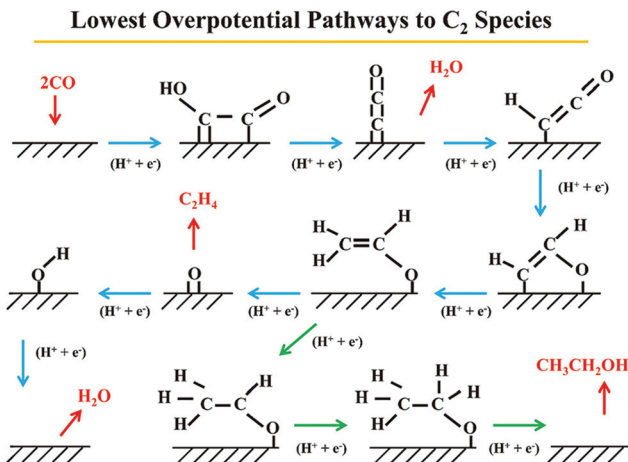


Fig. 14 Lowest free energy pathway of CO_2 electroreduction to C_2H_4 and $\text{C}_2\text{H}_5\text{OH}$ [reproduced with permission from ref. 83. Copyright (2013) WILEY-VCH Verlag GmbH & Co. KGaA, Weinheim].

more favorable at high overpotentials. Contradictory to their conclusions, Koper *et al.*, who observed high C_2H_4 catalytic activity of the Cu electrode experimentally,^{81,82} argued that the CO coupling step proceeded *via* CO^* interacting with a non-adsorbed CO molecule on Cu(100), and only needed to overcome a 0.52 eV small barrier to form $\text{CO}-\text{CO}^*$ dimer species with electron and proton transfer decoupled at -0.40 eV,⁸³ the typical onset potential for ethylene production. C_2H_4 was further hydrogenated from $\text{CO}-\text{CO}^*$ under several typical PCET steps (Fig. 14). Their results were in better agreement with their experimental findings that only C_2H_4 was produced at low overpotentials and the C–C coupling step was pH independent.⁸² The CHE model, despite being inapplicable in C–C coupling steps, is still valid for PCET steps and provides reasonable agreement with experiments in C_2H_4 production.

To summarize in short, the CHE model has been proven to be effective in unraveling rate-determining PCET steps, regardless of the product type. The linear scaling relation between adsorption intermediates is able to simplify the complicated multiple PCET steps into single/double descriptor space volcano plots, providing opportunities to design novel cathodes that possess less negative overpotential and higher current density. Nevertheless, as discussed below, another kinetic model used in modeling practice provides different insights into several aspects such as the origin of the overpotential, the reaction intermediate.

3.2. Water solvated and shuttling model

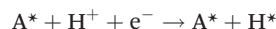
The above-mentioned theoretical investigations on CO_2 electrocatalysis to CO , CH_4 and C_2H_4 are all based on the purely thermodynamic CHE model, and the calculations were mainly performed just as those in a vacuum (solid–gas interface thermocatalysis). As alternatives to this thermodynamical approach with the empirical solvent correction term, many kinds of kinetic models that incorporate explicitly water molecules,

although to a limited extent, have been proposed in the literature.^{50,51,84,85} To the best of our knowledge, only two models have been utilized in CO_2 electro-reduction environments.

Shi *et al.* studied CO_2 electro-reduction on Pt(111) using an electronic double layer model.⁸⁶ In this model, a hexagonal water layer was put above the Pt(111) surface. In addition, a proton was added to one of the water molecules near the adsorbate. The function of the introduced proton was to induce charge separation between the metal surface and the water layer, simulating a double layer in reality. They found that from CO_2 to surface C^* species, the proton transfer barriers and C–O bond dissociation barriers were in the range of ~0.1 eV and ~0.5 eV, respectively. Such small barriers were easy to be surmounted, proving the validity of using the CHE model.

Nie *et al.* studied CO_2 electro-reduction on the Cu(111) surface employing a two-layer water model or inclusion of 1–2 water molecules.⁸⁷ However, they adopted a constant-potential approach⁸⁸ rather than the constant-charge method by Shi *et al.*⁸⁶ In this approach, a surface H^* adsorbed on Cu instead of a hydrated proton was used to represent a proton–electron couple. A PCET step $\text{A}^* + \text{H}^+ + \text{e}^- \rightarrow \text{B}^*$ was then replaced by: $\text{A}^* + \text{H}^* \rightarrow \text{B}^*$.

An equilibrium potential U_0 was calculated using the criterion that the free energy difference between both sides of the following reaction was zero:



Note that the free energy of the proton–electron couple at the left side is calculated in terms of that of $\frac{1}{2}\text{H}_2(\text{g})$ like in the CHE model.

Then, the calculated reaction barrier E_a^0 was extrapolated to different applied potentials U using the Butler–Volmer equation:⁸⁹

$$E_a(U) = E_a^0 + \beta(U - U_0)$$

where β is a symmetry factor which is approximated as 0.5.

Based on the potential-dependent reaction barrier, two models were proposed, namely, the solvated model and the shuttling model, as depicted in Fig. 15. In the former one, the adsorbed H^* directly reacted with reaction intermediates while in the latter one, H^* underwent shuttling through 1 or 2 water molecules and one of the water molecules transferred H to intermediates.

Nie *et al.*⁸⁹ suggested that CHO^* formation from CO^* was preferable *via* the solvated model, while COH^* was likely to be produced *via* the shuttling model. Furthermore, they found that CO^* to COH^* rather than CHO^* needed a less negative potential to make the hydrogenation surmountable (0.4 eV). COH^* then accepted a proton and removed a water molecule to become surface C^* species and subsequently the final product CH_4 (Fig. 15). The corresponding kinetic barriers were surmountable in an ambient water environment with an applied bias of -0.98 V, in quantitatively agreement with the experiment overpotential for an appreciable current density.⁸⁷

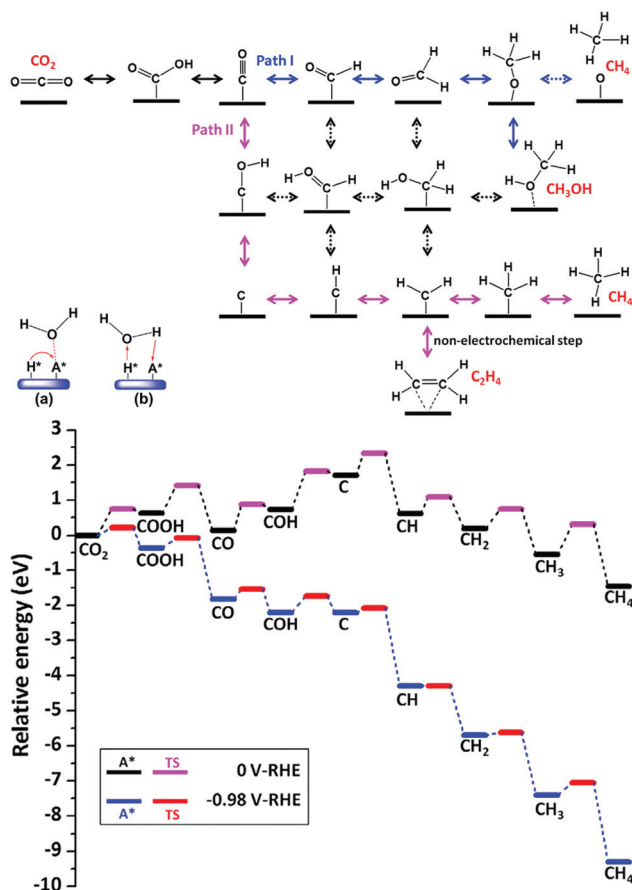


Fig. 15 Proposed reaction paths for CO₂ electrochemical reduction on Cu(111), schematic presentation of the solvated model (a) and the shuttling model (b), relative free energy diagrams for reaction path II through a COH* intermediate, at 0 and -0.98 V vs. RHE [adapted with permission from ref. 89. Copyright (2014) Elsevier Inc.].

In contrast, CH₃O* was preferentially reduced to CH₃OH *via* the H shuttling route, suggesting that CH₃O* would not be the intermediate for CH₄ production, thus further ruling out CHO* formation as the key intermediate. These studies highlight the importance of considering kinetic factors in solutions in a more comprehensive way when studying electrocatalysis with respect to solid–gas interface thermocatalysis.

3.3. Comparison with electrochemical experiments

Fig. 16 lists the routes for CHO* and COH* in CO₂ electrocatalysis to methane based on the CHE model and the water shuttling model, respectively. The thermodynamic CHE model and the kinetic water shuttling model both depict CO₂ electro-reduction on Cu quantitatively well. However, they exhibit notable discrepancy in several aspects. The electrochemical experiments showed that CO₂ and CO electro-reduction led to similar product distributions,^{46,47,90,91} suggesting that CO* was generated during CO₂ electro-reduction. Both the CHE model and the water shuttling model confirm the generation of CO as a crucial step during CO₂ electro-reduction because

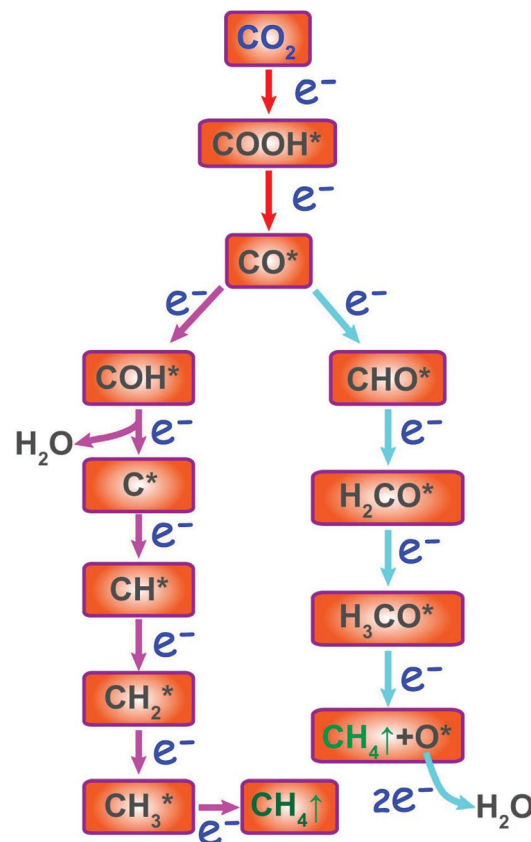


Fig. 16 CO₂ electrocatalysis to CH₄ on the Cu electrode *via* the COH* mechanism (pink arrows) or the CHO* mechanism (cyan arrows); e⁻ denotes electron transfer.

CO is both thermodynamically and kinetically favored. The discrepancy between the two models happens along the steps where CO undergoes further reduction. CHO* is identified as the key intermediate in the CHE model while COH* is believed in the water shuttling model. Their explanations of the origin of the overpotential are also different. In the CHE model, the origin of the overpotential comes from the most positive free energy change from CO* to CHO*.⁵² In the water shuttling model, it is the H shuttling barrier to generate COH* that determines the overpotential.⁸⁷

In gas phase thermocatalysis, although Cu is also used as the most effective catalyst, CH₃OH is the main product instead of CH₄. The origin of the difference of product distribution between electrocatalysis and gas phase thermocatalysis is also argued by the two models. In the CHE model, a more negative free energy gain in CH₄ production and the geometrical feasibility for proton transfer to the CH₃ moiety of OCH₃* are believed to be the cause of the overwhelming CH₄ production in liquid phase electrocatalysis.⁵² In the water shuttling model, the lower barrier for proton shuttling to the O atom of CO cannot happen in gas-phase thermocatalysis, leading to the difference of product distribution.⁸⁷ The experimental progress in characterizing CO₂ electro-reduction intermediates may provide useful insights into which mechanism is more conceivable.

CH_2O is the further reduction product of CHO^* in the CHE model. Electrokinetic experiments held by Hori *et al.*⁴⁵ and Schouten *et al.*⁸¹ both observed that CH_2O reduction mainly produces methanol and H_2 with a small amount of methane, which indicates that the formation of CH_2O will not occur in the dominant path of CO_2 or CO electro-reduction on Cu. Furthermore, DeWulf *et al.* observed a graphitic carbon species based on the X-ray photoelectron spectroscopy (XPS) and Auger electron spectroscopy (AES) performed *in situ* during CO_2 electro-reduction experiments.⁴⁶ These studies suggest that COH^* and further C^* generations from CO are more likely to happen, as illustrated by the water shuttling model, and that kinetics for proton transfer should not be entirely omitted.

4. Discussion and future outlook

We have reviewed recent theoretical advances in solid-gas thermocatalytic and solid-liquid electrocatalytic conversions of CO_2 to CO, CH_4 , CH_3OH , HCOOH , long chain hydrocarbons and alcohols based on the studies using density functional theory, KMC simulation, microkinetics modeling and different solvent models, which have been proven to be useful in catalyst design as well as in clarifications and corroborations of experimental mechanisms. However, challenges still remain to be overcome in many aspects including: (1) an explanation of the low yield of long-chain hydrocarbons and oxygenates is still lacking; (2) accurate description of CO_2 cannot be achieved by the traditional generalized gradient approximation (GGA) functional; (3) theoretical studies on semiconductor catalysts in solution are scarce, which is important in photo-electrochemical CO_2 conversion; (4) modeling methods need to be improved. More details will be given below.

4.1. Monocarbon product preference in thermocatalysis on Cu and further outlook for long chain carbon fuel production

For thermocatalytic CO_2 reduction on Cu-based catalysts, the monocarbon species constitute the main products. In contrast, CO/H_2 mixed gas is used industrially to produce long-chain hydrocarbons and oxygenates on dopant promoted Co- and Rh-based catalysts, respectively, namely Fischer-Tropsch (FT) synthesis.^{3,92} The distinct product distribution between CO_2 reduction and CO reduction motivates us to analyze why C-C coupling steps are hard to occur on Cu based catalysts.

In the forming HCOO process, CO_2 reduction shares the same route with CO after the formation of CH_2O^* ; thus, we first analyze the steps after CH_2O^* formation. If one wants to improve the yields of C_2 or C_n ($n > 2$) products, then there should be efficient C-C coupling steps after CH_2O^* formation. Unfortunately, this is not the case for Cu-based catalysts. Previous theoretical studies on Fischer-Tropsch synthesis on various metals have already found that CH_2O^* hydrogenation to CH_3OH on Cu is the most favorable.⁹³ In contrast, CH_xO ($x = 0-3$) dissociation to CH_x as well as CH_xO insertion to CH_x

need to surmount a much larger barrier on pure Cu.⁹⁴ These findings suggest that CO_2 reduction is not likely to give rise to C_2 or C_n ($n > 2$) products on Cu through the CO intermediate.

Next, we analyze the steps before CHO^* formation. The crucial intermediates before CHO^* formation are HCOO^* , H_2COO^* , HCOOH , and H_2COOH . C-bonding patterns are nearly saturated in these intermediates and thus these intermediates are not likely to couple with each other. Similar situations can also be found in the intermediates according to the *trans*- COOH^* mechanism. Therefore, regardless of steps before or after CH_2O^* formation, the C-C coupling steps are always unfavorable. That is why Cu-based catalysts tend to produce monocarbon species from CO_2/H_2 .

Based on the fact that HCOO^* , H_2COO^* , HCOOH , and H_2COOH are difficult to couple with each other or other intermediates, the most promising approach to achieve large-scale long chain carbon fuel production is modified FT synthesis, namely, generating CO first and producing long chain carbon fuel using CO as a feedstock. Therefore, to promote the synthesis of C_2 or C_n ($n > 2$) products (hydrocarbons and alcohols), future efforts should focus on discovering new catalysts that promotes CO generation from CO_2/H_2 , C-O bond dissociation from CH_xO and CO/CHO insertion to CH_x simultaneously. Experimentally, Fe-based catalysts have been identified to be promising for long-chain olefin generation.^{95,96} However, the catalysts are highly susceptible to deactivation from coking.⁹⁷ Furthermore, the catalyst activity was proved to be highly dependent on promoters (such as K)⁹⁸⁻¹⁰¹ substrates (Al_2O_3 , SiO_2)¹⁰¹⁻¹⁰³ as well as catalytic phases (Fe oxides and carbides).^{95,96} Similarly, Fe/Rh-based catalysts possess notable catalytic activity towards long chain alcohol formation with appropriate dopants and promoters.^{104,105} However, the selectivity is still relatively low and large amounts of CO intermediates generated from CO_2 reduction are consumed in the undesired methanation reaction.¹⁰⁴ Therefore, to optimize the catalyst performance, further theoretical efforts should be devoted to the area of CO_2 thermocatalytic reduction to long chain carbon fuels. Unfortunately, little attention has been paid to Fe-based catalysts in theoretical modeling, although a lot of theoretical studies aiming at traditional FT synthesis catalysts using CO as a feedstock have emerged in recent years.^{92,93,106-118} More theoretical investigations are needed to clarify the decisive factors in improving Fe-based catalyst performance and discover better catalysts, with the combination of experimental findings.

Furthermore, it is also important to note that although CO is a crucial intermediate in CO_2 thermocatalytic reduction to long chain carbon fuels, the product distribution varies a lot when using CO_2 instead of CO as a feedstock on certain catalysts. For example, Co-based catalysts that perform well in FT synthesis using CO as a feedstock are weak in transforming CO_2 to the desired hydrocarbons.¹⁰² Instead, methane becomes the main product even when Co is mixed with Fe or other elements.^{102,119} This implies that the adsorption properties of CO_2 might also need to be fully considered in theoretical modeling and simulations.

4.2. Difference between Cu-based CO₂ thermoreduction and electroreduction

To unveil why electrocatalytic CO₂ reduction leads to more C₂ species, one should first address the analogies and differences between solid–gas and solid–liquid CO₂ conversions. We have already discussed in section 3.3 that CO* is the crucial intermediate in electrocatalytic CO₂ reduction. Using the CHE model, Montoya *et al.* and Calle-Vallejo *et al.* identified 2CHO* coupling on Cu(211) and CO* coupling to CO(g) on Cu(100) as the rate-determining step, respectively.^{80,83} Moreover, Nie *et al.* identified 2CH₂* coupling on Cu(111) as the rate-determining step based on the water shuttling model.⁸⁹ Despite the fact that their studies were handled on different facets, there is one aspect shared by them that there are reaction steps either before C–C coupling or during C–C coupling that are controlled by the applied potential. The reaction barriers are able to be reduced with the applied potential becomes larger. Such potential-controlled reaction steps cannot be achieved in solid–gas thermocatalysis. That is why more C₂ and longer carbon chain products can be produced *via* CO₂ electroreduction on Cu, while Cu-based catalysts are much more likely to produce monocarbon products *via* CO₂ thermoreduction.

Based on the difference in the above-mentioned mechanism between CO₂ thermoreduction and electroreduction on Cu-based catalysts, it is obvious that the theoretical approach can be used to search for novel electrocatalysts that are capable of producing liquid fuels. CO* and OH* binding strengths are identified as the two most important factors in deciding product distribution and selectivity (especially for CH₃OH and CH₄ products).^{52,120} For instance, new alloy catalysts such as WAu were identified to possess high selectivity towards CH₃OH production with a careful consideration of OH* adsorption energies.¹²⁰

4.3. Deficiencies in theory and modeling & future directions

From sections 2 and 3 we can see that DFT plays a major role in suggesting possible catalytic mechanisms, finding reasonable elementary steps, giving insight into catalyst geometries, calculating energy barriers of certain surface reactions, and determining the theoretical overpotentials in both thermocatalytic and electrocatalytic CO₂ reduction. However, at the macroscopic length and time scale, statistical and empirical simulations are highly preferred in order to unravel the interplay between elementary chemical reactions that occurred under real-world operating conditions. KMC and microkinetics simulations have become representatives of such simulation methods in modelling CO₂ reduction in recent years, and they have often been utilized in combination with DFT to realize a multi-scale investigation.

On real-world catalytic surfaces, the reactants, intermediates and products adsorb and desorb continuously. One aspect that DFT cannot tackle well is that the time between instantaneous elementary steps is much longer, which is called the rare-event dynamics.¹²¹ Furthermore, the interplay between different reactants, intermediates and products often happens

at a larger spatial scale than DFT that is capable of resolving. Atomistic scale KMC simulations, based on the statistical model and algorithm, combine the elementary processes and focus on their interplay statistically, with the aim of appropriately estimating the surface chemical kinetics. Therefore, KMC simulations are able to reveal the chemical composition, reactant/product distribution and expected activity parameters in a long period of simulation time, with the integration of accurately calculated first-principles calculated rate constants.

If the length and time scales are beyond the scope of both DFT and KMC, microkinetic modelling, one important part of continuum modelling, will instead be an ideal framework for integrating the data generated by DFT and KMC. Microkinetic modelling shares the same point with KMC that they both concentrate on product distribution and estimating the catalyst activity in steady state kinetics. However, distinct from the fact that KMC is operated in a relatively small time and length scale and that KMC includes all possible reaction paths without impurity, microkinetic modelling generally requires a particular reaction mechanism and paths in terms of the most elementary steps. Furthermore, the input data required to establish a microkinetic model are distributed more widely, often not only including first-principles, but also experiments. Due to its larger time and length scales, microkinetic modelling is more susceptible to mass transfer effects.¹²²

Combining DFT, KMC and microkinetic approaches makes the technical sense of multiscale modelling. The DFT data can be used as input parameters for larger scale atomistic simulation and continuum modelling, and the preferred structural parameters and intermediate geometries obtained at the steady state by KMC and microkinetics can in turn be better analyzed in detail by DFT. It has been proven to be very effective in many theoretical studies on CO₂ reduction.^{13,14,53} However, there are still some notable deficiencies in currently used theory and modeling methods. For thermocatalytic CO₂ reduction (especially to CH₃OH), DFT calculations can be used to search for the more probable reaction paths with relatively small energy barriers. Since the surface coverage of intermediates correlates closely with different mechanisms that existed in parallel, it would be more reasonable that the CO₂ heterogeneous reduction to methanol may proceed *via* various low-barrier paths with different probabilities. However, in practice, due to structural complexity of catalytic materials, only a small subset of reaction paths is chosen to reduce the computational cost in DFT computations, and the employed models such as extended^{12,13,29} or simple stepped⁵ or defected^{17,21} surfaces cannot be fully informative. Moreover, there are several intrinsic shortcomings of DFT methods in describing the energies of several reaction intermediates, for example: (1) overestimation or underestimation of CO and CO₂ adsorption energies on transition metal-based catalysts when using DFT instead of DFT+U, especially in semiconductors;^{76,77,123} (2) overestimation of CO₂ hydrogenation energy.¹⁵ These limitations also indicate the need to seek for the above-mentioned microkinetics modeling and the KMC method to complement the traditional DFT computations for addressing product

selectivity and reaction rates, not only for a wider time and length scale, but also for a better computational accuracy.

On the other hand, although KMC methods were claimed to be more accurate and reliable for heterogeneous catalytic reactions,^{15,124,125} the computational cost is too excessive. Microkinetics, superior in alleviating the computational cost, is insufficient to account for fluctuations and usually overestimates the surface adsorbate coverage because it assumes intermediates diffusing and contacting with the solid phase in an optimum manner, which is usually not the case. However, microkinetics modeling is more effective and can still give turnover frequencies (TOFs) that are in qualitative agreement with those given by KMC. More information can be found in ref. 63, 64, 126–130. Particularly, Brønsted–Evans–Polanyi (BEP) relationships⁶⁴ are helpful in giving linear correlations between adsorption energies of transition states and those of reaction intermediates; and the Sabatier principle¹²⁷ is fundamental to the volcano plot. The combination of these two would result in a universal scaling relationship as well as thermodynamic activity volcanoes, which have been proven to give an excellent agreement between theory and experiment data in many heterogeneous catalytic processes.^{131,132} Although volcano plots and microkinetics have been adopted in CO thermocatalytic conversion¹³² and CO₂ electrocatalytic conversion,⁵³ we have not found similar practices applied to CO₂ thermocatalytic conversion. It is therefore of great promise to apply volcano plots and microkinetics analysis for better CO₂ heterogeneous catalyst design.

In CO₂ electrocatalysis, there are also several challenges in theory and modeling: (1) modeling of the semiconductor–liquid interface and electrolytes that assist in electron injection to CO₂ remains to be scarce.^{74,133–135} Most of the current theoretical studies focus merely on metal cathodes, paying little attention to semiconductors as well as the chemical composition and effect of electrolytes. The explicit charge–counter-charge solvated models such as those used in the double-reference method contain much more solvent molecules and are often accurate enough to describe the effect of solvation and electrode potential. However, the computation costs in these explicit models are too demanding. Furthermore, to date only PCET steps have been intensively investigated, without the consideration of other kinds of induced electron transfers such as photoeffect. Future research on photo-electrochemical CO₂ reduction and using less solvent molecules to achieve a tradeoff between accuracy and computational cost will be beneficial in designing more efficient catalytic materials. (2) Surface morphology effect is largely omitted. Nie *et al.* have claimed that with respect to different facets of the Cu cathode, the relative stability between CHO* and COH* intermediates can be reversed.⁸⁹ Furthermore, electrochemical tests by Schouten *et al.* also revealed that the onset potential is almost equal between CH₄ and C₂H₄ synthesis on Cu(111), while it is much smaller for C₂H₄ production on Cu(100).⁸² Detailed investigation of surface morphology might give explanations of the above-mentioned discrepancies between the CHE model and the water shuttling model applied to different facets in

section 3.3, corroborating the rationality of both models. (3) Input geometries might also influence final results significantly. For instance, in the water shuttling model, the activation barrier of COOH* generation from CO₂ depends largely on the input geometry. Zhao *et al.* used a bent CO₂ initial geometry with strong interaction with Cu(111) and proposed the *trans*-COOH mechanism.²⁹ However, Nie *et al.* claimed that the linear CO₂ molecule weakly adsorbed on Cu(111) was more stable than the bent configuration and that actually H* transfer to CO₂ to generate COOH* had a much larger barrier.⁸⁹ A similar conclusion has also been drawn on Cu₂O(111) by Bendavid *et al.*¹²³ It is never too important to scrutinize the most stable initial geometry configurations in future theoretical studies. (4) Extending successful approaches in handling other electrochemical processes into CO₂ electrocatalytic reduction. It would be worthy to note that in the field of ORR and HER electrocatalysis, many theoretical studies focused on the nature of the solid–liquid interface.^{85,136,137} These techniques of modeling complex solid–liquid interfaces (such as the double reference method¹³⁶) are highly desirable in the field of CO₂ electrocatalysis with the advancement of computational resources. Therefore, to explore the mechanisms of CO₂ electrocatalysis in depth, we believe that it would be worth paying attention to the following aspects in the future research: (1) an electrochemical phase diagram as a function of the applied potential;¹³⁶ (2) the modified Poisson–Boltzmann approach for Tafel lines generation;¹³⁸ (3) constant-charge or constant-potential, which is better in modeling the electrolyte–catalyst interface (electrochemical double layer); (4) cyclic voltammetry curves simulation using KMC methods;¹³⁹ (5) unifying the thermodynamic and kinetic volcanoes.¹⁴⁰ Although these methods or models have been employed in ORR and HER, applications to CO₂ electro-reduction have not been reported due to a complicated electron process involved in electrocatalysis. So, using multiple methods to synergistically elucidate the reaction mechanisms and pathways of CO₂ electro-reduction will be of paramount interest for future research.

Acknowledgements

This work was partially supported by grants from the National Research Foundation (NRF) of Singapore under its Campus for Research Excellence and Technological Enterprise (CREATE) programme and from the National Natural Science Foundation of China (NSFC-21173007, 11274023), as well as from the National Grand Fundamental Research 973 Program of China (2012CB921404).

Notes and references

- D. Cheng, F. R. Negreiros, E. Aprà and A. Fortunelli, *Chem-SusChem*, 2013, 6, 944–965.
- Q. Ge, in *New and Future Developments in Catalysis*, ed. S. L. Suib, Elsevier, Amsterdam, 2013, pp. 49–79.

- 3 W. Wang, S. Wang, X. Ma and J. Gong, *Chem. Soc. Rev.*, 2011, **40**, 3703–3727.
- 4 X.-M. Liu, G. Q. Lu, Z.-F. Yan and J. Beltramini, *Ind. Eng. Chem. Res.*, 2003, **42**, 6518–6530.
- 5 M. Behrens, F. Studt, I. Kasatkin, S. Kühl, M. Hävecker, F. Abild-Pedersen, S. Zander, F. Girgsdies, P. Kurr, B.-L. Kniep, M. Tovar, R. W. Fischer, J. K. Nørskov and R. Schlögl, *Science*, 2012, **336**, 893–897.
- 6 J. C. J. Bart and R. P. A. Sneeden, *Catal. Today*, 1987, **2**, 1–124.
- 7 J. Yoshihara, S. C. Parker, A. Schafer and C. Campbell, *Catal. Lett.*, 1995, **31**, 313–324.
- 8 J. Yoshihara and C. T. Campbell, *J. Catal.*, 1996, **161**, 776–782.
- 9 T. Fujitani, I. Nakamura, T. Uchijima and J. Nakamura, *Surf. Sci.*, 1997, **383**, 285–298.
- 10 T. Kakumoto, *Energy Convers. Manage.*, 1995, **36**, 661–664.
- 11 T. Kakumoto and T. Watanabe, *Catal. Today*, 1997, **36**, 39–44.
- 12 Y. Yang, J. Evans, J. A. Rodriguez, M. G. White and P. Liu, *Phys. Chem. Chem. Phys.*, 2010, **12**, 9909–9917.
- 13 L. C. Grabow and M. Mavrikakis, *ACS Catal.*, 2011, **1**, 365–384.
- 14 Q.-L. Tang, Q.-J. Hong and Z.-P. Liu, *J. Catal.*, 2009, **263**, 114–122.
- 15 Q.-J. Hong and Z.-P. Liu, *Surf. Sci.*, 2010, **604**, 1869–1876.
- 16 Q. Sun and Z. Liu, *Front. Chem. China*, 2011, **6**, 164–172.
- 17 S. A. French, A. A. Sokol, S. T. Bromley, C. R. A. Catlow, S. C. Rogers, F. King and P. Sherwood, *Angew. Chem., Int. Ed.*, 2001, **40**, 4437–4440.
- 18 J. Ye, C. Liu and Q. Ge, *J. Phys. Chem. C*, 2012, **116**, 7817–7825.
- 19 J. Ye, C. Liu, D. Mei and Q. Ge, *ACS Catal.*, 2013, **3**, 1296–1306.
- 20 Y.-x. Pan, C.-j. Liu and Q. Ge, *J. Catal.*, 2010, **272**, 227–234.
- 21 J. Xiao and T. Frauenheim, *J. Phys. Chem. Lett.*, 2012, **3**, 2638–2642.
- 22 P. A. Taylor, P. B. Rasmussen and I. Chorkendorff, *J. Chem. Soc., Faraday Trans.*, 1995, **91**, 1267–1269.
- 23 Y. Yang, M. G. White and P. Liu, *J. Phys. Chem. C*, 2011, **116**, 248–256.
- 24 E. Vesselli, E. Monachino, M. Rizzi, S. Furlan, X. Duan, C. Dri, A. Peronio, C. Africh, P. Lacovig, A. Baldereschi, G. Comelli and M. Peressi, *ACS Catal.*, 2013, **3**, 1555–1559.
- 25 J. Nerlov and I. Chorkendorff, *Catal. Lett.*, 1998, **54**, 171–176.
- 26 J. Nerlov and I. Chorkendorff, *J. Catal.*, 1999, **181**, 271–279.
- 27 P. Liu, Y. Choi, Y. Yang and M. G. White, *J. Phys. Chem. A*, 2009, **114**, 3888–3895.
- 28 A. J. Elliott, R. A. Hadden, J. Tabatabaei, K. C. Waugh and F. W. Zemicael, *J. Catal.*, 1995, **157**, 153–161.
- 29 Y.-F. Zhao, Y. Yang, C. Mims, C. H. F. Peden, J. Li and D. Mei, *J. Catal.*, 2011, **281**, 199–211.
- 30 S. Yin and Q. Ge, *Catal. Today*, 2012, **194**, 30–37.
- 31 B. Chan and L. Radom, *J. Am. Chem. Soc.*, 2006, **128**, 5322–5323.
- 32 B. Chan and L. Radom, *J. Am. Chem. Soc.*, 2008, **130**, 9790–9799.
- 33 G.-C. Wang and J. Nakamura, *J. Phys. Chem. Lett.*, 2010, **1**, 3053–3057.
- 34 C. Liu, T. R. Cundari and A. K. Wilson, *J. Phys. Chem. C*, 2012, **116**, 5681–5688.
- 35 E. Vesselli, L. D. Rogatis, X. Ding, A. Baraldi, L. Savio, L. Vattuone, M. Rocca, P. Fornasiero, M. Peressi, A. Baldereschi, R. Rosei and G. Comelli, *J. Am. Chem. Soc.*, 2008, **130**, 11417–11422.
- 36 E. Vesselli, M. Rizzi, L. De Rogatis, X. Ding, A. Baraldi, G. Comelli, L. Savio, L. Vattuone, M. Rocca, P. Fornasiero, A. Baldereschi and M. Peressi, *J. Phys. Chem. Lett.*, 2009, **1**, 402–406.
- 37 H. Tominaga and M. Nagai, *Appl. Catal., A*, 2005, **282**, 5–13.
- 38 J. A. Rodriguez, J. Evans, L. Feria, A. B. Vidal, P. Liu, K. Nakamura and F. Illas, *J. Catal.*, 2013, **307**, 162–169.
- 39 G. Peng, S. J. Sibener, G. C. Schatz, S. T. Ceyer and M. Mavrikakis, *J. Phys. Chem. C*, 2011, **116**, 3001–3006.
- 40 G. Peng, S. J. Sibener, G. C. Schatz and M. Mavrikakis, *Surf. Sci.*, 2012, **606**, 1050–1055.
- 41 Q. Zhang, L. Cao, B. Li and L. Chen, *Chem. Sci.*, 2012, **3**, 2708–2715.
- 42 J. S. Yoo, F. Abild-Pedersen, J. K. Nørskov and F. Studt, *ACS Catal.*, 2014, **4**, 1226–1233.
- 43 Y. Hori, K. Kikuchi and S. Suzuki, *Chem. Lett.*, 1985, **14**, 1695–1698.
- 44 Y. Hori, K. Kikuchi, A. Murata and S. Suzuki, *Chem. Lett.*, 1986, **15**, 897–898.
- 45 Y. Hori, A. Murata and R. Takahashi, *J. Chem. Soc., Faraday Trans. 1*, 1989, **85**, 2309–2326.
- 46 D. W. DeWulf, T. Jin and A. J. Bard, *J. Electrochem. Soc.*, 1989, **136**, 1686–1691.
- 47 J. J. Kim, D. P. Summers and K. W. Frese Jr., *J. Electroanal. Chem. Interfacial Electrochem.*, 1988, **245**, 223–244.
- 48 Y. Hori, A. Murata, K. Kikuchi and S. Suzuki, *J. Chem. Soc., Chem. Commun.*, 1987, 728–729.
- 49 J. K. Nørskov, J. Rossmeisl, A. Logadottir, L. Lindqvist, J. R. Kitchin, T. Bligaard and H. Jónsson, *J. Phys. Chem. B*, 2004, **108**, 17886–17892.
- 50 M. J. Janik, C. D. Taylor and M. Neurock, *J. Electrochem. Soc.*, 2009, **156**, B126–B135.
- 51 V. Tripković, E. Skúlason, S. Siahrostami, J. K. Nørskov and J. Rossmeisl, *Electrochim. Acta*, 2010, **55**, 7975–7981.
- 52 A. A. Peterson, F. Abild-Pedersen, F. Studt, J. Rossmeisl and J. K. Nørskov, *Energy Environ. Sci.*, 2010, **3**, 1311–1315.
- 53 H. A. Hansen, J. B. Varley, A. A. Peterson and J. K. Nørskov, *J. Phys. Chem. Lett.*, 2013, **4**, 388–392.
- 54 Y. Chen and M. W. Kanan, *J. Am. Chem. Soc.*, 2012, **134**, 1986–1989.
- 55 C. W. Li and M. W. Kanan, *J. Am. Chem. Soc.*, 2012, **134**, 7231–7234.

- 56 C. W. Li, J. Ciston and M. W. Kanan, *Nature*, 2014, **508**, 504–507.
- 57 X. Nie, G. L. Griffin, M. J. Janik and A. Asthagiri, *Catal. Commun.*, 2014, **52**, 88–91.
- 58 M. Le, M. Ren, Z. Zhang, P. T. Sprunger, R. L. Kurtz and J. C. Flake, *J. Electrochem. Soc.*, 2011, **158**, E45–E49.
- 59 A. A. Peterson and J. K. Nørskov, *J. Phys. Chem. Lett.*, 2012, **3**, 251–258.
- 60 C. Shi, H. A. Hansen, A. C. Lausche and J. K. Nørskov, *Phys. Chem. Chem. Phys.*, 2014, **16**, 4720–4727.
- 61 Y.-J. Zhang, V. Sethuraman, R. Michalsky and A. A. Peterson, *ACS Catal.*, 2014, **4**, 3742–3748.
- 62 M. Karamad, V. Tripkovic and J. Rossmeisl, *ACS Catal.*, 2014, **4**, 2268–2273.
- 63 J. K. Nørskov, T. Bligaard, A. Logadottir, S. Bahn, L. B. Hansen, M. Bollinger, H. Bengaard, B. Hammer, Z. Sljivancanin, M. Mavrikakis, Y. Xu, S. Dahl and C. J. H. Jacobsen, *J. Catal.*, 2002, **209**, 275–278.
- 64 T. Bligaard, J. K. Nørskov, S. Dahl, J. Matthiesen, C. H. Christensen and J. Sehested, *J. Catal.*, 2004, **224**, 206–217.
- 65 W. J. Durand, A. A. Peterson, F. Studt, F. Abild-Pedersen and J. K. Nørskov, *Surf. Sci.*, 2011, **605**, 1354–1359.
- 66 D.-H. Lim, J. H. Jo, D. Y. Shin, J. Wilcox, H. C. Ham and S. W. Nam, *Nanoscale*, 2014, **6**, 5087–5092.
- 67 W. Zhu, R. Michalsky, Ö. Metin, H. Lv, S. Guo, C. J. Wright, X. Sun, A. A. Peterson and S. Sun, *J. Am. Chem. Soc.*, 2013, **135**, 16833–16836.
- 68 K. Manthiram, B. J. Beberwyck and A. P. Alivisatos, *J. Am. Chem. Soc.*, 2014, **136**, 13319–13325.
- 69 R. Reske, H. Mistry, F. Behafarid, B. Roldan Cuenya and P. Strasser, *J. Am. Chem. Soc.*, 2014, **136**, 6978–6986.
- 70 A. Parkin, J. Seravalli, K. A. Vincent, S. W. Ragsdale and F. A. Armstrong, *J. Am. Chem. Soc.*, 2007, **129**, 10328–10329.
- 71 J. B. Varley, H. A. Hansen, N. L. Ammitzbøll, L. C. Grabow, A. A. Peterson, J. Rossmeisl and J. K. Nørskov, *ACS Catal.*, 2013, **3**, 2640–2643.
- 72 K. Chan, C. Tsai, H. A. Hansen and J. K. Nørskov, *ChemCatChem*, 2014, **6**, 1899–1905.
- 73 C. Tsai, K. Chan, J. K. Nørskov and F. Abild-Pedersen, *J. Phys. Chem. Lett.*, 2014, **5**, 3884–3889.
- 74 M. Asadi, B. Kumar, A. Behrangiinia, B. A. Rosen, A. Baskin, N. Repnin, D. Pisasale, P. Phillips, W. Zhu, R. Haasch, R. F. Klie, P. Král, J. Abiade and A. Salehi-Khojin, *Nat. Commun.*, 2014, **5**, DOI: 10.1038/ncomms5470.
- 75 H.-K. Lim, H. Shin, W. A. Goddard, Y. J. Hwang, B. K. Min and H. Kim, *J. Am. Chem. Soc.*, 2014, **136**, 11355–11361.
- 76 I. M. B. Nielsen and K. Leung, *J. Phys. Chem. A*, 2010, **114**, 10166–10173.
- 77 K. Leung, I. M. B. Nielsen, N. Sai, C. Medforth and J. A. Shelnutt, *J. Phys. Chem. A*, 2010, **114**, 10174–10184.
- 78 E. Fujita, C. Creutz, N. Sutin and D. J. Szalda, *J. Am. Chem. Soc.*, 1991, **113**, 343–353.
- 79 V. Tripkovic, M. Vanin, M. Karamad, M. E. Björketun, K. W. Jacobsen, K. S. Thygesen and J. Rossmeisl, *J. Phys. Chem. C*, 2013, **117**, 9187–9195.
- 80 J. H. Montoya, A. A. Peterson and J. K. Nørskov, *ChemCatChem*, 2013, **5**, 737–742.
- 81 K. J. P. Schouten, Y. Kwon, C. J. M. van der Ham, Z. Qin and M. T. M. Koper, *Chem. Sci.*, 2011, **2**, 1902–1909.
- 82 K. J. P. Schouten, Z. Qin, E. P. Gallent and M. T. M. Koper, *J. Am. Chem. Soc.*, 2012, **134**, 9864–9867.
- 83 F. Calle-Vallejo and M. T. M. Koper, *Angew. Chem., Int. Ed.*, 2013, **52**, 7282–7285.
- 84 C. D. Taylor, S. A. Wasileski, J.-S. Filhol and M. Neurock, *Phys. Rev. B: Condens. Matter*, 2006, **73**, 165402.
- 85 E. Skúlason, V. Tripkovic, M. E. Björketun, S. d. Gudmundsdóttir, G. Karlberg, J. Rossmeisl, T. Bligaard, H. Jónsson and J. K. Nørskov, *J. Phys. Chem. C*, 2010, **114**, 18182–18197.
- 86 C. Shi, C. P. O’Grady, A. A. Peterson, H. A. Hansen and J. K. Nørskov, *Phys. Chem. Chem. Phys.*, 2013, **15**, 7114–7122.
- 87 X. Nie, M. R. Esopi, M. J. Janik and A. Asthagiri, *Angew. Chem., Int. Ed.*, 2013, **52**, 2459–2462.
- 88 S. A. Wasileski and M. J. Janik, *Phys. Chem. Chem. Phys.*, 2008, **10**, 3613–3627.
- 89 X. Nie, W. Luo, M. J. Janik and A. Asthagiri, *J. Catal.*, 2014, **312**, 108–122.
- 90 M. Gattrell, N. Gupta and A. Co, *J. Electroanal. Chem.*, 2006, **594**, 1–19.
- 91 Y. Hori, A. Murata, R. Takahashi and S. Suzuki, *J. Am. Chem. Soc.*, 1987, **109**, 5022–5023.
- 92 Y.-H. Zhao, K. Sun, X. Ma, J. Liu, D. Sun, H.-Y. Su and W.-X. Li, *Angew. Chem., Int. Ed.*, 2011, **50**, 5335–5338.
- 93 Y. Choi and P. Liu, *J. Am. Chem. Soc.*, 2009, **131**, 13054–13061.
- 94 R. Zhang, G. Wang, B. Wang and L. Ling, *J. Phys. Chem. C*, 2014, **118**, 5243–5254.
- 95 T. Riedel, H. Schulz, G. Schaub, K.-W. Jun, J.-S. Hwang and K.-W. Lee, *Top. Catal.*, 2003, **26**, 41–54.
- 96 H. Schulz, T. Riedel and G. Schaub, *Top. Catal.*, 2005, **32**, 117–124.
- 97 S.-C. Lee, J.-S. Kim, W. C. Shin, M.-J. Choi and S.-J. Choung, *J. Mol. Catal. A: Chem.*, 2009, **301**, 98–105.
- 98 M. Niemelä and M. Nokkosmäki, *Catal. Today*, 2005, **100**, 269–274.
- 99 W. Ning, N. Koizumi and M. Yamada, *Energy Fuels*, 2009, **23**, 4696–4700.
- 100 H. Arakawa and A. T. Bell, *Ind. Eng. Chem. Proc. Des. Dev.*, 1983, **22**, 97–103.
- 101 G. Zhao, C. Zhang, S. Qin, H. Xiang and Y. Li, *J. Mol. Catal. A: Chem.*, 2008, **286**, 137–142.
- 102 T. Riedel, M. Claeys, H. Schulz, G. Schaub, S.-S. Nam, K.-W. Jun, M.-J. Choi, G. Kishan and K.-W. Lee, *Appl. Catal., A*, 1999, **186**, 201–213.
- 103 S.-R. Yan, K.-W. Jun, J.-S. Hong, M.-J. Choi and K.-W. Lee, *Appl. Catal., A*, 2000, **194–195**, 63–70.

- 104 T. Inui, T. Yamamoto, M. Inoue, H. Hara, T. Takeguchi and J.-B. Kim, *Appl. Catal., A*, 1999, **186**, 395–406.
- 105 H. Kusama, K. Okabe, K. Sayama and H. Arakawa, *Catal. Today*, 1996, **28**, 261–266.
- 106 J. Cheng, P. Hu, P. Ellis, S. French, G. Kelly and C. M. Lok, *J. Phys. Chem. C*, 2008, **112**, 9464–9473.
- 107 O. R. Inderwildi, S. J. Jenkins and D. A. King, *J. Phys. Chem. C*, 2008, **112**, 1305–1307.
- 108 Z.-J. Zuo, L. Wang, L.-M. Yu, P.-D. Han and W. Huang, *J. Phys. Chem. C*, 2014, **118**, 12890–12898.
- 109 T. H. Pham, X. Duan, G. Qian, X. Zhou and D. Chen, *J. Phys. Chem. C*, 2014, **118**, 10170–10176.
- 110 L. Joos, I. A. W. Filot, S. Cottenier, E. J. M. Hensen, M. Waroquier, V. Van Speybroeck and R. A. van Santen, *J. Phys. Chem. C*, 2014, **118**, 5317–5327.
- 111 R. A. van Santen, A. J. Markvoort, M. M. Ghouri, P. A. J. Hilbers and E. J. M. Hensen, *J. Phys. Chem. C*, 2013, **117**, 4488–4504.
- 112 C.-F. Huo, Y.-W. Li, J. Wang and H. Jiao, *J. Am. Chem. Soc.*, 2009, **131**, 14713–14721.
- 113 B. T. Loveless, C. Buda, M. Neurock and E. Iglesia, *J. Am. Chem. Soc.*, 2013, **135**, 6107–6121.
- 114 A. Tuxen, S. Carencio, M. Chintapalli, C.-H. Chuang, C. Escudero, E. Pach, P. Jiang, F. Borondics, B. Beberwyck, A. P. Alivisatos, G. Thornton, W.-F. Pong, J. Guo, R. Perez, F. Besenbacher and M. Salmeron, *J. Am. Chem. Soc.*, 2013, **135**, 2273–2278.
- 115 R. A. van Santen, A. J. Markvoort, I. A. W. Filot, M. M. Ghouri and E. J. M. Hensen, *Phys. Chem. Chem. Phys.*, 2013, **15**, 17038–17063.
- 116 R. A. van Santen, M. M. Ghouri, S. Shetty and E. M. H. Hensen, *Catal. Sci. Technol.*, 2011, **1**, 891–911.
- 117 F. Li, D.-E. Jiang, X. C. Zeng and Z. Chen, *Nanoscale*, 2012, **4**, 1123–1129.
- 118 R. A. van Santen, M. Ghouri and E. M. J. Hensen, *Phys. Chem. Chem. Phys.*, 2014, **16**, 10041–10058.
- 119 F. Tihay, A. C. Roger, G. Pourroy and A. Kiennemann, *Energy Fuels*, 2002, **16**, 1271–1276.
- 120 S. Back, H. Kim and Y. Jung, *ACS Catal.*, 2014, **5**, 965–971.
- 121 K. Reuter, in *Modeling Heterogeneous Catalytic Reactions: From the Molecular Process to the Technical System*, ed. O. Deutschmann, Wiley-VCH, 2011, pp. 71–111.
- 122 L. J. Broadbelt and R. Q. Snurr, *Appl. Catal., A*, 2000, **200**, 23–46.
- 123 L. I. Bendavid and E. A. Carter, *J. Phys. Chem. C*, 2013, **117**, 26048–26059.
- 124 R. M. Ziff, E. Gulari and Y. Barshad, *Phys. Rev. Lett.*, 1986, **56**, 2553–2556.
- 125 B. Temel, H. Meskine, K. Reuter, M. Scheffler and H. Metiu, *J. Chem. Phys.*, 2007, **126**, 204711.
- 126 A. A. Gokhale, S. Kandoi, J. P. Greeley, M. Mavrikakis and J. A. Dumesic, *Chem. Eng. Sci.*, 2004, **59**, 4679–4691.
- 127 J. K. Nørskov, T. Bligaard, J. Rossmeisl and C. H. Christensen, *Nat. Chem.*, 2009, **1**, 37–46.
- 128 J. K. Nørskov, F. Abild-Pedersen, F. Studt and T. Bligaard, *Proc. Natl. Acad. Sci. U. S. A.*, 2011, **108**, 937–943.
- 129 J. Hafner, C. Wolverton and G. Ceder, *MRS Bull.*, 2006, **31**, 659–668.
- 130 B. Hammer and J. K. Nørskov, in *Advances in Catalysis*, ed. H. K. Bruce and C. Gates, Academic Press, 2000, vol. 45, pp. 71–129.
- 131 M. P. Andersson, T. Bligaard, A. Kustov, K. E. Larsen, J. Greeley, T. Johannessen, C. H. Christensen and J. K. Nørskov, *J. Catal.*, 2006, **239**, 501–506.
- 132 F. Studt, F. Abild-Pedersen, Q. Wu, A. D. Jensen, B. Temel, J.-D. Grunwaldt and J. K. Nørskov, *J. Catal.*, 2012, **293**, 51–60.
- 133 M. Z. Ertem, S. J. Konezny, C. M. Araujo and V. S. Batista, *J. Phys. Chem. Lett.*, 2013, **4**, 745–748.
- 134 J. A. Keith and E. A. Carter, *J. Phys. Chem. Lett.*, 2013, **4**, 4058–4063.
- 135 A. B. Muñoz-García and E. A. Carter, *J. Am. Chem. Soc.*, 2012, **134**, 13600–13603.
- 136 J.-S. Filhol and M. Neurock, *Angew. Chem., Int. Ed.*, 2006, **45**, 402–406.
- 137 F. Calle-Vallejo and M. T. M. Koper, *Electrochim. Acta*, 2012, **84**, 3–11.
- 138 Y.-H. Fang and Z.-P. Liu, *J. Am. Chem. Soc.*, 2010, **132**, 18214–18222.
- 139 V. Viswanathan, H. A. Hansen, J. Rossmeisl, T. F. Jaramillo, H. Pitsch and J. K. Nørskov, *J. Phys. Chem. C*, 2012, **116**, 4698–4704.
- 140 H. A. Hansen, V. Viswanathan and J. K. Nørskov, *J. Phys. Chem. C*, 2014, **118**, 6706–6718.